Hole scattering and optical transitions in wide-band-gap nitrides: Wurtzite and zinc-blende structures

Yu. M. Sirenko, J. B. Jeon, B. C. Lee, K. W. Kim, and M. A. Littlejohn
Department of Electrical and Computer Engineering, North Carolina State University, Raleigh, North Carolina 27695-7911

M. A. Stroscio and G. J. Iafrate
U. S. Army Research Office, Post Office Box 12211, Research Triangle Park, North Carolina 27709-2211

(Received 15 July 1996)

The energy spectrum and transitions of valence-band carriers in wurtzite materials are studied theoretically using cubic crystals for comparison. We correct the commonly used cubic approximation and propose notations for Luttinger-like parameters in wurtzite structures that simplify the cubic approximation to $\gamma_{1z}=\gamma_{1\perp}$, $\gamma_{2z}=\gamma_{2\perp}$, and $\gamma_{3z}=\gamma_{3\perp}$. We establish the relation between two recently proposed 3×3 matrix blocks diagonalizing the full 6×6 Hamiltonian and provide geometric interpretation in three-dimensional Bloch space. The formalism is used then to derive transition matrix elements for three types of processes: (i) macrofield hole scattering, described by the Bloch overlap factor; (ii) optical transitions between conduction and valence bands; and (iii) intervalence band optical transitions. Finally, we discuss the set of material parameters for group-III nitrides and present the numerical results. [S0163-1829(97)08207-6]

I. INTRODUCTION

Interest in the material properties and applications of wide-band-gap III-V semiconductors has grown rapidly in the past several years. Direct band group-III nitride semiconductors, such as GaN, AlN, InN, and their alloys, possess superior characteristics that should produce reliable, high-performance devices.[1–4] Progress achieved in high-quality GaN growth on buffered sapphire substrates[5] and *p*-type doping[6] has led to high-quality *p-n* homo- and heterojunctions[7] that are the basis for numerous optoelectronic device applications (green to UV light-emitting diodes,[8] lasers,[9] and solar-blind photodetectors[10]) as well as high-power electronic devices.[11]

Despite technology advances and commercial applications of group-III nitrides, many of the fundamental material properties are poorly understood and further experimental and theoretical studies are required. Major experimental efforts are devoted to the analysis of optical properties,[12] defects,[13] and transport phenomena[14] in GaN-based materials. On the other hand, a number of empirical and *ab initio* methods have been applied for calculating the full Brillouin zone energy spectra, optical and structural properties of group-III nitrides and their alloys,[15,16] as well as mobility[17] and light emission[18] in these materials. Although the wide-band-gap nitride materials are grown in both zinc-blende (cubic) and wurtzite (hexagonal) polytypes, the wurtzite structure is predominant for the device applications.

As for other direct band-gap group-III-V compounds, many important optical and transport properties of GaN-based materials are determined by carriers near $\mathbf{k}=\mathbf{0}$ in the small vicinity of the Γ point. Conduction-band states for small wave vector $\mathbf{k}$ are doubly degenerate with respect to spin and can be characterized by one or two (for cubic or hexagonal symmetries) energy-independent effective masses. The valence-band spectrum near the Γ point is more complicated and originates from the sixfold degenerate Γ_{15} state (see Fig. 1). In zinc-blende structures, the spin-orbit interaction splits the Γ_{15} level at $\mathbf{k}=\mathbf{0}$, forming the fourfold degenerate Γ_8 (heavy and light holes) and doubly degenerate Γ_7 (spin split-off holes) levels. Joint action of the hexagonal component of crystal field and the spin-orbit interaction in wurtzite crystals leads to the formation of three distinct levels: Γ_9, upper Γ_7, and lower Γ_7, which we denote as HH (heavy holes), LH (light holes), and SH (split-off holes), respectively. For normal valence-band order, as shown on Fig. 1, these states correspond to the *A*-, *B*-, and *C*-type exciton lines in photoluminescence experiments.

The description of spectra and transitions in the vicinity of the Γ point involving three (doubly degenerate) valence bands is conveniently achieved in an envelope-function formalism.[19,20] For *cubic* symmetry, the spectrum and eigenstates of holes in a strained crystal are determined by a 6×6 matrix Luttinger-Kohn-Bir-Pikus[19,21,22] (LKBP) Hamiltonian, and in *hexagonal* crystals with the C_{6v} point symmetry group, the Rashba-Sheka-Pikus[19,23,24] (RSP) 6×6 matrix Hamiltonian should be utilized. The envelope-

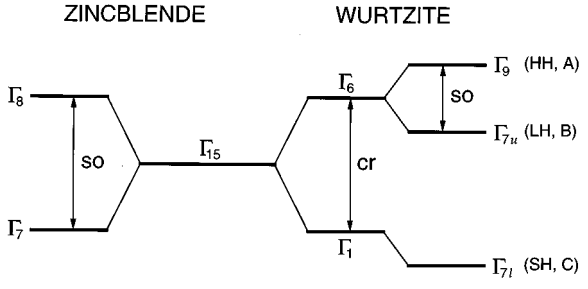

FIG. 1. Valence-band structure in zinc-blende and wurtzite crystals at the Γ point. In cubic materials levels Γ_8 and Γ_7 are separated due to the spin-orbit interaction. In wurtzite structures the levels Γ_9, Γ_{7u} (upper), and Γ_{7l} (lower) are formed due to the action of the spin-orbit interaction and the hexagonal component of crystal field.

function method uses the most general form of the Hamiltonian allowed by the crystal symmetry, which depends on a number of empirical material constants. The LKBP cubic Hamiltonian is specified by 7 empirical constants: spin-orbit splitting energy Δ_{so}, Luttinger parameters $\gamma_{1,2,3}$, and deformation potential constants a_v, b, and d. However, for the strained wurtzite crystal, as many as 16 independent constants are required for use of the RSP Hamiltonian:[19] splitting energies $\Delta_{1,2,3}$, band-curvature parameters A_1–A_6, strain-related constants D_1–D_6, and a factor A_7 for the linear in wave-vector term.

The cubic Hamiltonian has been applied extensively to a large number of problems involving holes in group-IV and -III-V materials; yet, until recently, the RSP Hamiltonian has been used mainly for describing excitons in group-II-VI hexagonal structures.[25–30] Very recently, the RSP Hamiltonian has been applied to analyze the valence-band spectra in hexagonal GaN and related materials.[31–36] Using data from experiments and from first-principles calculations, the hole energy spectrum in bulk GaN and other wurtzite materials was obtained,[31] including the effects of strain.[34–36] Different diagonalization forms for the full 6×6 Hamiltonian have been proposed[32–34] and the results applied to calculate dispersion of holes in unstrained[32] and strained[33,36] $Al_xGa_{1-x}N$/GaN quantum wells. It was pointed out[31–36] that the quasicubic approximation for wurtzite structures[19,26,37] is an important tool for the estimation of experimentally unavailable parameters.

In this paper we discuss properties of the RSP Hamiltonian, the quasicubic approximation, and we calculate the matrix elements for hole scattering and optical transitions in wurtzite materials, keeping close analogy to the cubic case. In Sec. II we revisit the quasicubic approximation for wurtzite materials and correct a mistake[38] in its frequently used form.[19] The correction only changes signs of Bir and Pikus's parameters A_5 and A_6; thus it does not affect any results for hole wave vector $\mathbf{k}$ either parallel or perpendicular to the c axis. In view of the importance of analogy between cubic and wurtzite materials, we propose to use, instead of constants A_1–A_6, the set Luttinger-like parameters with the built-in quasicubic relation: $\gamma_{1z}=\gamma_{1\perp}$, $\gamma_{2z}=\gamma_{2\perp}$, and $\gamma_{3z}=\gamma_{3\perp}$. Section III discusses the properties of two forms[32–34] proposed for 3×3 blocks of the RSP Hamiltonian and shows that they are related by a simple rotation around the heavy-hole axis in the three-dimensional Bloch function space.

Section IV deals with the derivation of transition matrix elements for hole scattering and optical processes using the block-diagonalized forms of the RSP Hamiltonian for strained wurtzite crystals. More specifically, Sec. IV A contains the calculation of Bloch overlap factor for holes scattered by a macrofield. In Sec. IV B the matrix elements of valence-band to conduction-band transitions are calculated in the dipole approximation for an arbitrary polarization of light. Section IV C describes intervalence-band optical transitions in strained bulk wurtzite materials. As the limiting cases, the corresponding expressions for the cubic crystal (with warping neglected) are reproduced. Finally, Sec. V contains our conclusions and the Appendixes detail parts of the calculations.

II. ZINC-BLENDE AND WURTZITE VALENCE-BAND HAMILTONIANS

The envelope-function description of valence bands in the vicinity of the Γ point in cubic and hexagonal materials can be conveniently achieved within an invariant method[22,24] for construction of the hole Hamiltonian H. In this method the Hamiltonian is written in terms of combinations in different powers of hole wave-vector components and external perturbations[19,26] (strain, magnetic, and electric fields) allowed by the crystal symmetry. A broad class of physical problems of interest can be described by a Hamiltonian containing terms up to the second order in wave vector $\mathbf{k}$ and linear in strain tensor ε:

$$H(\mathbf{k},\varepsilon)=H_0+H_{\mathbf{k}}+H_{\varepsilon}+\cdots. \tag{1}$$

In both cubic and hexagonal materials the top six valence bands originate from p^3 orbitals (corresponding to the vector representation Γ_{15}; see Fig. 1) split by the spin-orbit interaction and/or hexagonal crystal field. Therefore, it is convenient to express the corresponding 6×6 Hamiltonian in Eq. (1) as a direct product of 3×3 matrices $(L_x,L_y,L_z)\equiv\mathbf{L}$ of angular momentum 1 and the 2×2 Pauli matrices[39] $(\sigma_x,\sigma_y,\sigma_z)\equiv\boldsymbol{\sigma}$ of spin 1/2.

A. Cubic structures

The invariant form of the LKBP 6×6 Hamiltonian for cubic crystals is given by Eq. (1) with[19]

$$H_0^{\mathrm{cub}}=\frac{\Delta_{so}}{3}(\mathbf{L}\cdot\boldsymbol{\sigma}),$$

$$\begin{aligned}H_{\mathbf{k}}^{\mathrm{cub}}=&-(\gamma_1+4\gamma_2)k^2+6\gamma_2(\mathbf{L}\cdot\mathbf{k})^2+6(\gamma_3-\gamma_2)\\&\times(2[L_xL_y]k_xk_y+\mathrm{c.p.}),\end{aligned} \tag{2}$$

$$\begin{aligned}H_{\varepsilon}^{\mathrm{cub}}=&(a_v+2b)(\varepsilon_{xx}+\varepsilon_{yy}+\varepsilon_{zz})-(3bL_x^2\varepsilon_{xx}+\mathrm{c.p.})\\&-\sqrt{3}d(2[L_xL_y]\varepsilon_{xy}+\mathrm{c.p.}).\end{aligned}$$

Here Δ_{so} is the spin-orbit splitting energy, γ_1, γ_2, and γ_3 are Luttinger parameters (for simplicity, we omitted factor $\hbar^2/2m_0$), a_v, b, and d are Bir-Pikus valence-band deformation potential constants, and $2[L_iL_j]\equiv L_iL_j+L_jL_i$. Terms not containing matrices L or σ are assumed to be multiplied by 3×3 or 2×2 unity matrices. The relations between parameters $\gamma_1,\gamma_2,\gamma_3$ (deformation potentials a_v,b,d) and other common sets are given in Appendix A.

B. Hexagonal structures

In wurtzite materials, the 6×6 matrix form of the RSP Hamiltonian for the top valence bands is given by Eq. (1) and[19,24]

$$H_0^{\mathrm{wur}}=\Delta_1L_z^2+\Delta_2L_z\sigma_z+\sqrt{2}\Delta_3(L_+\sigma_-+L_-\sigma_+),$$

$$\begin{aligned}H_{\mathbf{k}}^{\mathrm{wur}}=&A_1k_z^2+A_2k_\perp^2+(A_3k_z^2+A_4k_\perp^2)L_z^2\\&+A_5(L_+^2k_-^2+L_-^2k_+^2)+A_6k_z(2[L_zL_+]k_-\\&+2[L_zL_-]k_+)+iA_7(L_+k_--L_-k_+),\end{aligned}$$

$$H_{\varepsilon}^{\mathrm{wur}}=D_1\varepsilon_{zz}+D_2\varepsilon_{\perp}+(D_3\varepsilon_{zz}+D_4\varepsilon_{\perp})L_z^2 + D_5(L_+^2\varepsilon_-+L_-^2\varepsilon_+)+D_6(2[L_zL_+]\varepsilon_{-z} + 2[L_zL_-]\varepsilon_{+z}). \quad (3)$$

Here the z axis is chosen along the [0001] direction (c axis); $k_{\perp}^2=k_x^2+k_y^2$, $k_{\pm}=k_x\pm ik_y$, $\varepsilon_{\perp}=\varepsilon_{xx}+\varepsilon_{yy}$, $\varepsilon_{\pm z}=\varepsilon_{xz}\pm i\varepsilon_{yz}$, and $\varepsilon_{\pm}=\varepsilon_{xx}-\varepsilon_{yy}\pm 2i\varepsilon_{xy}$. In Eq. (3) we use the notation of Pikus[24,27] for the ladder operators[40] $L_{\pm}$ and $\sigma_{\pm}$,

$$L_{\pm}=(L_x\pm iL_y)/\sqrt{2}, \quad \sigma_{\pm}=(\sigma_x\pm i\sigma_y)/2.$$

The RSP Hamiltonian in Eqs. (1) and (3) describes the top valence bands in strained wurtzite materials with 16 empirical constants: Δ_1–Δ_3, A_1–A_7, and D_1–D_6. Here $\Delta_1\equiv\Delta_{\mathrm{cr}}$ is a splitting energy due to the hexagonal component of crystal field;[37] $\Delta_{\mathrm{so}}^{(z)}\equiv 3\Delta_2$ and $\Delta_{\mathrm{so}}^{(\perp)}\equiv 3\Delta_3$ are spin-orbit splitting energies for z and perpendicular directions.

Parameters A_1–A_6 determine (together with splitting energies Δ_i) direction-dependent effective masses in unstrained crystals. To elucidate the analogy existing between valence bands in cubic and hexagonal crystals and to facilitate the use of the cubic approximation for wurtzite structures, we introduce the set of Luttinger-like parameters γ:

$$-A_1=\gamma_{1z}+4\gamma_{3z}, \quad -A_2=\gamma_{1\perp}-2\gamma_{3\perp}, \quad A_3=6\gamma_{3z}, \quad -A_4=3\gamma_{3\perp}, \quad A_5=\gamma_{2\perp}+2\gamma_{3\perp}, \quad A_6=\sqrt{2}(2\gamma_{2z}+\gamma_{3z}). \quad (4)$$

We omitted the factor $\hbar^2/2m_0$ in Eq. (4) to simplify the relation between dimensionless constants γ and parameters A. In a similar fashion, we define constants δ, related to deformation potentials D:

$$-D_1=\delta_{1z}+4\delta_{3z}, \quad -D_2=\delta_{1\perp}-2\delta_{3\perp}, \quad D_3=6\delta_{3z}, \quad -D_4=3\delta_{3\perp}, \quad D_5=\delta_{2\perp}+2\delta_{3\perp}, \quad D_6=\sqrt{2}(2\delta_{2z}+\delta_{3z}). \quad (5)$$

We note the following correspondence between terms in $H_{\mathbf{k}}$ and H_{ε}:

$$\frac{\hbar^2}{2m_0}\gamma_{iz,\perp}k_{\alpha}k_{\beta} \leftrightarrow \delta_{iz,\perp}\varepsilon_{\alpha\beta}. \quad (6)$$

Finally, the factor for the term linear in $k_{\perp}$ of Eq. (3) can be presented as

$$A_7=\hbar^2k_s/m_0, \quad (7)$$

where k_s characterizes the radius of the circular loop of valence-band maxima[28] reached at $k_z=0$ and finite $k_{\perp}$.

C. Cubic approximations

In contrast to zinc-blende materials where the description of top valence bands requires four (seven in the case of strain) empirical parameters, wurtzite structures are described by ten (sixteen in the presence of strain) material constants. Such a large number of material constants is unlikely to be determined reliably from experiment alone; thus certain empirical relations such as quasicubic[19,27,26,29,37] or spherical cubic[33] approximations are required. The physical background for the cubic approximation stems from the similar arrangements of neighboring atoms in cubic and hexagonal materials: the first coordination sphere in the wurtzite lattice can be obtained from the cubic one by applying a relatively small deformation in the [111] direction.

A comparison of corresponding terms in Eq. (3) for wurtzite structures and the cubic Hamiltonian in Eq. (2), transformed to the wurtzitelike coordinate frame, leads to several conditions, constituting the *quasicubic approximation*[37,19] (see Appendix B). First, the longitudinal and transverse spin-orbit splitting parameters are equal and correspond to the splitting energy for cubic crystals,

$$\Delta_2=\Delta_3\rightarrow\Delta_{\mathrm{so}}/3. \quad (8)$$

Second, in the quasicubic approximation there exist only three independent parameters in the $\gamma_{iz,\perp}$ set, corresponding to well-known Luttinger parameters γ_i for cubic structures [cf. Eq. (B6) for parameters A]:

$$\gamma_{1z}=\gamma_{1\perp}\rightarrow\gamma_1, \quad \gamma_{2z}=\gamma_{2\perp}\rightarrow\gamma_2, \quad \gamma_{3z}=\gamma_{3\perp}\rightarrow\gamma_3. \quad (9)$$

Similar relations hold between deformation potentials $\delta_{iz,\perp}$ and constants[19] a_v, b, and d of cubic materials:

$$\delta_{1z}=\delta_{1\perp}\rightarrow -a_v, \quad \delta_{2z}=\delta_{2\perp}\rightarrow -b/2, \quad \delta_{3z}=\delta_{3\perp}\rightarrow -d/2\sqrt{3}. \quad (10)$$

Finally, the cubic valence-band Hamiltonian in Eq. (2) lacks terms linear in the wave vector. Therefore, in the quasicubic approximation,

$$A_7\propto k_s\rightarrow 0. \quad (11)$$

It should be noted that, since the wurtzite symmetry point group C_{6v} is not a subgroup of the zinc-blende group T_d, there exist terms in the cubic Hamiltonian [see Eq. (B5) in Appendix B] that do not have counterparts in the wurtzite Hamiltonian in Eq. (3). Therefore the quasicubic approximation for Luttinger-like parameters γ and deformation potential constants δ, given in Eqs. (9) and (10), should be considered as empirical relations only.[19,26,27]

The wurtzite invariant Hamiltonian in Eq. (3) can be reduced to the cubic invariant in Eq. (2) only if the warping terms in Eq. (B5) are absent, i.e., if $\gamma_2\approx\gamma_3$ and $b\approx d/\sqrt{3}$. In the corresponding *spherical cubic approximation*[33] two relations are added to Eqs. (9) and (10) of the quasicubic approximation:

$$\gamma_{2z}=\gamma_{2\perp}=\gamma_{3z}=\gamma_{3\perp}\rightarrow\gamma_2, \quad (9')$$

$$\delta_{2z}=\delta_{2\perp}=\delta_{3z}=\delta_{3\perp}\rightarrow -b/2. \quad (10')$$

Thus, in the spherical cubic approximation a physically reasonable description of valence bands in strained wurtzite crystals is achieved with just six parameters: crystal field and spin-orbit splitting energies, Δ_{cr} and Δ_{so}, Luttinger-like parameters γ_1 and γ_2, as well as deformation potential constants a_v and b.

D. Crystal field as additional strain

The cubic Hamiltonian in Eq. (2) lacks terms corresponding to crystal splitting, i.e., Δ_{cr} in Eq. (3). Therefore, strictly speaking, in the cubic approximation the crystal field split-

ting should be set to zero, $\Delta_{cr}\to 0$. However, this approximation is qualitatively wrong for the description of wurtzite structures (e.g., it merges levels Γ_9 and Γ_{7u}); thus finite Δ_{cr} is preserved to account for the deviation from cubic symmetry.

The effect of nonzero crystal splitting nevertheless can be introduced rigorously into the cubic approximation by means of an ''additional'' deformation, described by a strain tensor ε^{add}. Inspecting terms H_0^{wur} and H_ε^{wur} of Eq. (3), proportional to the matrix operator L_z^2, we find that the crystal splitting parameter can be accounted for by the combination

$$\Delta_{cr}\to D_3\varepsilon_{zz}^{add}+D_4\varepsilon_\perp^{add}\approx 3b(\varepsilon_\perp^{add}/2-\varepsilon_{zz}^{add}). \tag{12}$$

Here the z axis corresponds to the [111] direction in cubic crystals. On the right-hand side of Eq. (12) we used the spherical cubic approximation for deformation potentials D, given by Eqs. (10′) and (5).

Since the additional strain must not contribute to other terms in Eq. (3), the tensor $\varepsilon\equiv\varepsilon^{add}$ should describe a *biaxial* deformation with

$$\varepsilon_{xx}=\varepsilon_{yy}\equiv\varepsilon_\perp/2,\quad \varepsilon_{xy}=\varepsilon_{yz}=\varepsilon_{xz}=0\,. \tag{13}$$

The remaining part of the additional strain contribution in Eq. (3), $(D_1\varepsilon_{zz}^{add}+D_2\varepsilon_\perp^{add})I$, leads to an overall shift of all valence bands and can be eliminated by the choice of energy reference.

It is of interest to determine the condition under which the ''internal'' strain in Eq. (12) can be represented as that in a layer pseudomorphically grown along the z axis. Substituting the relation between strain components in wurtzite crystals (where C_{ij} is a stiffness tensor),[41]

$$\varepsilon_{zz}=-(C_{13}/C_{33})\varepsilon_\perp\,, \tag{14}$$

into Eq. (12), we find

$$\left.\begin{matrix}\varepsilon_{xx}^{add}\\ =\varepsilon_{yy}^{add}\\ -\varepsilon_{zz}^{add}\end{matrix}\right\}=\frac{\Delta_{cr}}{3b}\left\{\begin{matrix}C_{33}\\ 2C_{13}\end{matrix}\right\}\Bigg/\,(C_{33}+2C_{13}). \tag{15}$$

Thus the correspondence between the hexagonal crystal field and additional strain established in Eq. (12) shows that wurtzite crystals are already ''prestrained'' in comparison to cubic ones and the external strain leads mainly to quantitative changes in the spectrum.

III. BLOCK-DIAGONAL HAMILTONIAN FORMS

Valence-band Hamiltonians for cubic and hexagonal structures are presented in Eqs. (1)–(3) in invariant, operator form. Using matrix representations of operators of angular momenta 1 and 1/2, $\mathbf{L}$ and $\boldsymbol{\sigma}$, in their corresponding bases,[40] one can obtain 6×6 matrix Hamiltonians H for describing three (doubly degenerate at $\mathbf{k}=\mathbf{0}$) top valence bands.[24,19,31,33]

As shown by Broido and Sham,[42] the 4×4 Luttinger-Kohn Hamiltonian can be diagonalized, by means of a unitary transformation, to two 2×2 nonzero blocks. This result has been subsequently generalized for a 6×6 LKBP cubic Hamiltonian describing coupled heavy-, light-, and spin split-off hole bands.[43]

Very recently, several different forms for the block-diagonalized wurtzite valence-band Hamiltonians have been proposed.[32–34] For biaxial strain specified by Eq. (13), the full 6×6 RSP Hamiltonian can be transformed, by an appropriate choice of basis functions, to the form

$$H=(\Delta_1+\Delta_2)I+\begin{bmatrix}H_+ & 0\\ 0 & H_-\end{bmatrix}. \tag{16}$$

The diagonal term $(\Delta_1+\Delta_2)I$ conveniently shifts to zero the eigenenergies of $H_\pm$, corresponding to heavy holes at $\mathbf{k}=\mathbf{0}$ (i.e., level Γ_9).

In the following we demonstrate the correspondence between different representations[33,34] proposed for 3×3 blocks $H_\pm$ and provide an explicit form of rotation for the Bloch function basis, which transforms one representation to another. Though the two forms of $H_\pm$ are equivalent to each other, one set of basis functions[33] diagonalizes the spin-orbit interaction (and should be used for comparison with cubic structures where $\Delta_{cr}\to 0$), while another basis function set[32,34] diagonalizes the hexagonal crystal field (and is convenient for an analysis of the nonrelativistic limit).

In the following we use the notation $|J,M\rangle$ for Bloch functions that behave, under symmetry operations of the point group, in the same way as eigenfunctions of an angular momentum J and its projection M on the z axis. Since the point group is only a subset of the full spherical symmetry group, the functions $|J,M\rangle$ do not constitute a representation of the latter. For simplicity, the spin-1/2 eigenfunctions are denoted by $|\uparrow\rangle$ and $|\downarrow\rangle$, while the orbital part of the conduction-band Bloch function is written as $|S\rangle$.

A. Cubiclike Hamiltonian

It is well known[19] that the basis function set $|\frac{3}{2},\pm\frac{3}{2}\rangle$, $|\frac{3}{2},\pm\frac{1}{2}\rangle$, and $|\frac{1}{2},\pm\frac{1}{2}\rangle$ diagonalizes the spin-orbit interaction term in Eq. (2). Thus it is convenient for the representation of the 6×6 Hamiltonian in *cubic* crystals. Therefore, to utilize the analogy existing between zinc-blende and cubic structures, we define the block-diagonalizing transformation[33] in a manner similar to the cubic case:[42,43]

$$\begin{aligned}|u_1,\pm\rangle_\varphi&=\frac{1}{\sqrt{2}}\left[\left|\frac{3}{2},\frac{3}{2}\right\rangle e^{-3i\varphi/2}\mp i\left|\frac{3}{2},-\frac{3}{2}\right\rangle e^{3i\varphi/2}\right],\\ |u_2,\pm\rangle_\varphi&=\frac{1}{\sqrt{2}}\left[\pm i\left|\frac{3}{2},\frac{1}{2}\right\rangle e^{-i\varphi/2}-\left|\frac{3}{2},-\frac{1}{2}\right\rangle e^{i\varphi/2}\right],\\ |u_3,\pm\rangle_\varphi&=\frac{1}{\sqrt{2}}\left[\pm i\left|\frac{1}{2},\frac{1}{2}\right\rangle e^{-i\varphi/2}+\left|\frac{1}{2},-\frac{1}{2}\right\rangle e^{i\varphi/2}\right].\end{aligned} \tag{17}$$

Here six basis states $|u_i,\sigma\rangle$ are numerated by symbols u_1, u_2, u_3, and the ''spin'' variable $\sigma=\pm$, assigning the state to the Bloch subspace of 3×3 Hamiltonians H_+ and H_-. The variable σ does not correspond to the actual particle spin; in fact, the definition of $\sigma\equiv\sigma_\varphi$ depends on the choice of basis in Eq. (17). For a finite perpendicular component of wave vector $\mathbf{k}_\perp$, the block-diagonalizing transformation in Eq. (17) depends on the angle $\varphi=\varphi_{\mathbf{k}}\equiv\arctan k_y/k_x$.

By applying the unitary transformation in Eq. (17), the 6×6 wurtzite Hamiltonian is presented in the block-diagonal form of Eq. (16). Denoting the terms linear in $k_\perp$ by H', we find the 3×3 upper and lower Hamiltonian blocks:

$$H_{\pm}=\pm H'-\begin{bmatrix} P+Q & R\mp iS & \sqrt{2}R\pm iS/\sqrt{2} \\ R\pm iS & P-Q & \sqrt{2}(Q+\Delta')\pm i\sqrt{\frac{3}{2}}S \\ \sqrt{2}R\mp iS/\sqrt{2} & \sqrt{2}(Q+\Delta')\mp i\sqrt{\frac{3}{2}}S & P+\Delta_{\rm so} \end{bmatrix} \begin{matrix} |u_1,\pm\rangle \\ |u_2,\pm\rangle \\ |u_3,\pm\rangle. \end{matrix} \tag{18}$$

Here

$$P=\frac{\Delta_{\rm cr}+2\Delta'}{3}+\gamma_{1z}k_z^2+\gamma_{1\perp}k_\perp^2+\delta_{1z}\varepsilon_{zz}+\delta_{1\perp}\varepsilon_\perp,$$

$$Q=-\frac{\Delta_{\rm cr}+2\Delta'}{3}-2\gamma_{3z}k_z^2+\gamma_{3\perp}k_\perp^2-2\delta_{3z}\varepsilon_{zz}+\delta_{3\perp}\varepsilon_\perp, \tag{19}$$

$$R=\sqrt{3}\overline{\gamma_\perp}k_\perp^2,\quad S=2\sqrt{3}\overline{\gamma_z}k_zk_\perp,$$

where $\overline{\gamma_\perp}\equiv(\gamma_{2\perp}+2\gamma_{3\perp})/3=A_5/3$ and $\overline{\gamma_z}\equiv(2\gamma_{2z}+\gamma_{3z})/3=A_6/3\sqrt{2}$; the isotropic spin-splitting energy $\Delta_{\rm so}=\Delta_2+2\Delta_3$ and its trigonal component[29] $\Delta'=\Delta_2-\Delta_3$. As for terms linear in $k_\perp$, they are given by the matrix

$$H'=\frac{T}{3}\begin{bmatrix} 0 & -\sqrt{6} & \sqrt{3} \\ -\sqrt{6} & -\sqrt{8} & -1 \\ \sqrt{3} & -1 & \sqrt{8} \end{bmatrix},$$

where

$$T=\hbar^2k_sk_\perp/m_0. \tag{19'}$$

We note that the rotation of the basis in Eq. (17) is not the only possible unitary transformation leading to block diagonalization of the valence-band Hamiltonian. However, the basis $|u_i,\sigma\rangle$ in Eq. (17) leads to the form Eq. (18), maximally close to the standard result for cubic structures.[42,43] In the absence of the hexagonal crystal field and strain, the matrix in Eq. (18) becomes diagonal at $\mathbf{k}=\mathbf{0}$ and basis states $|u_1,\sigma\rangle$, $|u_2,\sigma\rangle$, and $|u_3,\sigma\rangle$ coincide with the Bloch functions for heavy, light, and split-off holes.

B. Non-relativistic-like Hamiltonian

Consider the opposite case of fully diagonalized (at $\mathbf{k}_\perp=\mathbf{0}$) crystal-field contribution and nondiagonalized spin-orbit interaction. Taking the product of eigenfunctions of orbital momentum 1 and spin 1/2 as a basis in the transformation similar to Eq. (17) and using the Clebsch-Gordan relations in Appendix C for the basis change, we find

$$\begin{aligned} |u_1,\pm\rangle&=|v_1,\pm\rangle, \\ |u_2,\pm\rangle&=\frac{1}{\sqrt{3}}|v_2,\pm\rangle-\sqrt{\frac{2}{3}}|v_3,\pm\rangle, \\ |u_3,\pm\rangle&=\sqrt{\frac{2}{3}}|v_2,\pm\rangle+\frac{1}{\sqrt{3}}|v_3,\pm\rangle, \end{aligned} \tag{20}$$

where the new basis set $|v_i,\sigma\rangle$ is given by

$$\begin{aligned} |v_1,\pm\rangle_\varphi&=\frac{1}{\sqrt{2}}[|1,1\rangle|\uparrow\rangle e^{-3i\varphi/2}\mp i|1,-1\rangle|\downarrow\rangle e^{3i\varphi/2}], \\ |v_2,\pm\rangle_\varphi&=\frac{1}{\sqrt{2}}[\pm i|1,1\rangle|\downarrow\rangle e^{-i\varphi/2}-|1,-1\rangle|\uparrow\rangle e^{i\varphi/2}], \\ |v_3,\pm\rangle_\varphi&=\frac{1}{\sqrt{2}}[\mp i|1,0\rangle|\uparrow\rangle e^{-i\varphi/2}+|1,0\rangle|\downarrow\rangle e^{i\varphi/2}]. \end{aligned} \tag{21}$$

Applying the unitary transformation specified by Eq. (20) to the Hamiltonian in Eq. (18), we find the 3×3 block Hamiltonians in the basis of functions $|v_i,\sigma\rangle$:

$$H_{\pm}=-\begin{bmatrix} P+Q & \sqrt{3}R & \mp T\pm i\sqrt{\frac{3}{2}}S \\ \sqrt{3}R & P+Q+2\Delta_2 & \sqrt{2}\Delta_3\mp T\pm i\sqrt{\frac{3}{2}}S \\ \mp T\mp i\sqrt{\frac{3}{2}}S & \sqrt{2}\Delta_3\mp T\mp i\sqrt{\frac{3}{2}}S & P-2Q-\Delta_2+2\Delta_3 \end{bmatrix} \begin{matrix} |v_1,\pm\rangle \\ |v_2,\pm\rangle \\ |v_3,\pm\rangle. \end{matrix} \tag{22}$$

Here the terms P, Q, R, S, and T are defined in Eqs. (19) and (19′). The form (22) generalizes the result of Chuang and Chang[34] by including terms T linear in wave vector $k_\perp$.

At $\mathbf{k}_\perp=\mathbf{0}$, the only nondiagonal part of Hamiltonian (22) is due to the spin-orbit splitting term Δ_3. Thus, in the nonrelativistic approximation, the representation in Eqs. (21) and (22) provides the most convenient description of valence bands in wurtzite structures since the Bloch functions of heavy, light, and crystal-field split-off holes coincide with the basis vectors $|v_1,\sigma\rangle$, $|v_2,\sigma\rangle$, and $|v_3,\sigma\rangle$ at $\mathbf{k}_\perp=\mathbf{0}$.

For the general case of a finite spin-orbit interaction and hexagonal crystal field, there is no clear advantage of one of the forms in Eqs. (18) and (22) over the other. The cubiclike Hamiltonian in Eq. (18) is more convenient for using an analogy between cubic and wurtzite structures; however, the use of the non-relativistic-like Hamiltonian in Eq. (22) sometimes leads to simpler intermediate expressions. As will be demonstrated in Sec. III C, the two basis sets in Eqs. (17) and (21) are related to each other by a simple rotation in Bloch function space; thus they can be used interchangeably.

C. Spectrum and wave functions

The total carrier wave function can be presented as a linear combination of plane waves with defined momentum $\mathbf{k}$ and ''spin'' σ. For j-type holes (where j denotes a HH, LH, or SH) the total wave function $\Psi_{j\sigma\mathbf{k}}$ is equal to the product of the envelope $\exp(i\mathbf{k}\cdot\mathbf{r})$ and a periodic Bloch function $U_{j\sigma\mathbf{k}}$,

$$\Psi_{j\sigma\mathbf{k}}(\mathbf{r})=e^{i\mathbf{k}\cdot\mathbf{r}}U_{j\sigma\mathbf{k}}(\mathbf{r}). \tag{23}$$

In the envelope function method, the hole Bloch functions are presented, even at finite wave vector $\mathbf{k}$, as a linear combination of only six Γ-point Bloch functions. The latter can be taken as a direct product of three eigenfunctions of orbital angular momentum $L=1$ and two spinors. Thus the Bloch functions used in the envelope-function method, $\langle\mathbf{r}|j\sigma\mathbf{k}\rangle$, are the projections of the exact Bloch function $U_{j\sigma\mathbf{k}}$ on the subspace of functions with special symmetry properties corresponding to the Γ point. For finite $\mathbf{k}$, the exact Bloch functions deviate from their Γ-subspace component by a term proportional to a small wave vector $\mathbf{k}$:

$$U_{j\sigma\mathbf{k}}(\mathbf{r})=\langle\mathbf{r}|j\sigma\mathbf{k}\rangle+O(k). \tag{24}$$

The contribution of this term becomes important, even in the vicinity of the Γ point, if the matrix elements taken with zeroth-order terms $|j\sigma\mathbf{k}\rangle$ vanish due to symmetrical properties (see, e.g., the case of intervalence-band optical transitions in Sec. IV C).

Diagonalization of the valence-band Hamiltonian to two 3×3 blocks (for holes with opposite ''spin'' $\sigma=\pm$) simplifies the calculations in many cases of interest. This procedure also provides means for interpreting the Bloch functions $|j\sigma\mathbf{k}\rangle$ as vectors in three-dimensional Bloch spaces (see Fig. 2), spanned on basis functions in Eqs. (17) and (21). Using states $|u_i,\sigma\rangle$ as a basis, the Bloch states $|j\sigma\mathbf{k}\rangle$ can be written as

$$\begin{aligned}|j\sigma\mathbf{k}\rangle&=u^{(1)}_{j\mathbf{k}\sigma}|u_1,\sigma\rangle_\varphi+u^{(2)}_{j\mathbf{k}\sigma}|u_2,\sigma\rangle_\varphi+u^{(3)}_{j\mathbf{k}\sigma}|u_3,\sigma\rangle_\varphi\\&\equiv|\mathbf{u}_{\sigma\mathbf{k}}\rangle^{\mathrm{T}}\mathbf{u}_{j\mathbf{k}\sigma}.\end{aligned} \tag{25}$$

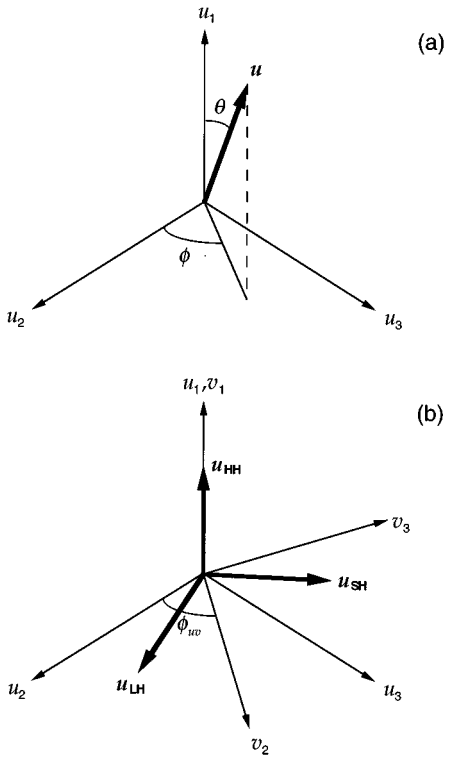

FIG. 2. Three-dimensional Bloch functions space. (a) Spherical coordinates θ and ϕ (in general, complex) of the Bloch vector $\mathbf{u}$. (b) Two coordinate frames u and v at an angle ϕ_{uv} from each other. At $k_\perp=0$, Bloch vectors of heavy holes (light and split-off holes) are real and directed along (perpendicular to) the axis $u_1=v_1$.

Here the set of basis vectors is given by $|\mathbf{u}_{\sigma\mathbf{k}}\rangle^{\mathrm{T}}=[|u_1,\sigma\rangle_\varphi,|u_2,\sigma\rangle_\varphi,|u_3,\sigma\rangle_\varphi]$, where the subscript $\varphi=\varphi_{\mathbf{k}}\equiv\arctan(k_y/k_x)$ shows explicitly that the basis states $|u_i,\sigma\rangle$ depend on the direction of wave vector $\mathbf{k}$.

The Bloch vector $\mathbf{u}_{j\mathbf{k}\sigma}$ of the j-type hole with spin σ and momentum $\mathbf{k}$ is specified by its three coordinates in the basis $|u_i,\sigma\rangle$. For the case where terms linear in $k_\perp$ can be neglected, the Bloch vectors of the opposite spins are related as $\mathbf{u}_{j\mathbf{k}+}=\mathbf{u}^*_{j\mathbf{k}-}\equiv\mathbf{u}_{j\mathbf{k}}$, i.e., the spin index σ can be dropped.

Normalizing vector $\mathbf{u}_{j\mathbf{k}}$ to unity, one can write

$$\mathbf{u}_{j\mathbf{k}}=\begin{bmatrix}u^{(1)}_{j\mathbf{k}}\\u^{(2)}_{j\mathbf{k}}\\u^{(3)}_{j\mathbf{k}}\end{bmatrix}\equiv\begin{bmatrix}\cos\theta_{j\mathbf{k}}\\\cos\phi_{j\mathbf{k}}\sin\theta_{j\mathbf{k}}\\\sin\phi_{j\mathbf{k}}\sin\theta_{j\mathbf{k}}\end{bmatrix}. \tag{26}$$

The right-hand side of Eq. (26) defines complex spherical coordinates ϕ and θ of unit vector $\mathbf{u}$ in the three-dimensional Bloch space spanned on the basis vectors $|u_i,\sigma\rangle$. Use of two complex angles ϕ and θ instead of three complex coordinates eliminates the possibility of multiplying $\mathbf{u}$ by an arbitrary complex constant and allows characterizing the complex (real) Bloch vector by only four (two) real numbers instead of six (three). The Bloch vectors are real for the case of wave vector $\mathbf{k}$ directed along the z axis (i.e., $k_\perp=0$).

In a similar fashion, the coordinate frame of basis vectors $|v_i,\sigma\rangle$ is introduced. As follows from Eq. (20) and Fig. 2(b), the v frame coincides with the u frame after rotation of the

angle $\phi_{uv}=\arctan\sqrt{2}\approx 55°$ around the common axis 1. Coordinates of Bloch vectors in both representations are simply related:

$$\theta^{(u)}=\theta^{(v)},\quad \phi^{(u)}=\phi^{(v)}+\phi_{uv}. \tag{27}$$

For each value of wave vector $\mathbf{k}$ and spin index σ, the 3×3 matrix Hamiltonians in Eq. (18) or (22) define three mutually orthogonal vectors $\mathbf{u}_{\mathrm{HH}}$, $\mathbf{u}_{\mathrm{LH}}$, and $\mathbf{u}_{\mathrm{SH}}$, corresponding to heavy, light, and split-off holes. For the arbitrary direction of $\mathbf{k}$, the calculation of the valence-band spectrum and Bloch vectors requires solution of a cubic equation.[33]

In the particular case of a wave vector parallel to the c axis, $k_\perp=0$, the heavy-hole state is decoupled from the other states and the valence-band energies can be written as

$$\begin{aligned} E_{\mathrm{HH}}(k_z,0)&=-\mathcal{D}-(\gamma_{1z}-2\gamma_{3z})k_z^2,\\ E_{\mathrm{LH,SH}}(k_z,0)&=-\mathcal{D}'-(\gamma_{1z}+\gamma_{3z})k_z^2\\ &\quad\pm\sqrt{(3\gamma_{3z}k_z^2+\mathcal{D}'')^2+2\Delta_3^2}, \end{aligned} \tag{28}$$

where $\mathcal{D}=-(\Delta_1+\Delta_2)+(\delta_{1z}-2\delta_{3z})\varepsilon_{zz}+(\delta_{1\perp}+\delta_{3\perp})\varepsilon_\perp$, $\mathcal{D}'=(\Delta_2-\Delta_1)/2+(\delta_{1z}+\delta_{3z})\varepsilon_{zz}+(\delta_{1\perp}-\delta_{3\perp}/2)\varepsilon_\perp$, and $\mathcal{D}''=(\Delta_1-\Delta_2)/2+3\delta_{3z}\varepsilon_{zz}-(3\delta_{3\perp}/2)\varepsilon_\perp$. As shown in Fig. 2(b), the corresponding eigenvectors are real and given by

$$\theta_{\mathrm{HH}}=0,\quad \theta_{\mathrm{LH,SH}}=\pi/2,\quad \phi_{\mathrm{SH}}=\phi_{\mathrm{LH}}+\pi/2. \tag{29}$$

The angle ϕ of light holes $\phi_{\mathrm{LH}}^{(v)}$ in the basis of functions $|v_i,\sigma\rangle$ is given by

$$\sin 2\phi_{\mathrm{LH}}^{(v)}=-\frac{2^{3/2}\Delta_3}{E_{\mathrm{LH}}-E_{\mathrm{SH}}}. \tag{30}$$

From Eqs. (29) and (30) one can analyze the form of the Bloch functions at $\mathbf{k}=\mathbf{0}$ in two opposite limits of small and large ratio $\Delta_{\mathrm{cr}}/\Delta_{\mathrm{so}}$. In the *cubic* case, i.e., $E_{\mathrm{LH}}-E_{\mathrm{SH}}=3\Delta_3=\Delta_{\mathrm{so}}$, one has $\phi_{\mathrm{LH}}^{(u)}=\phi_{\mathrm{LH}}^{(v)}+\phi_{uv}=0$, and the basis vectors $|u_i,\sigma\rangle$ in Eq. (17) represent the pure Bloch functions of heavy, light, and spin-orbit split-off holes. In the *nonrelativistic* case, i.e., $\Delta_3=0$, we obtain $\phi_{\mathrm{LH}}^{(v)}=0$, and the basis vectors $|v_i,\sigma\rangle$ of Eq. (21) coincide with Bloch functions of heavy, light, and crystal-field split-off holes. For the general case of finite Δ_{so} and Δ_{cr}, Fig. 2(b) shows that the Γ-point Bloch function of heavy holes is still given by the pure function $|u_1,\sigma\rangle=|v_1,\sigma\rangle$, while that of light and split-off holes are given by a mix of the limiting cubic and nonrelativistic cases.

IV. TRANSITION MATRIX ELEMENTS

A. Hole scattering: Bloch overlap factor

Many important carrier scattering mechanisms involving interaction with a macrofield[44] (most notably, Coulomb impurity scattering and polar interaction with optical phonons) are characterized by an interaction Hamiltonian $\hat{V}_{\mathrm{int}}$ diagonal in the Bloch function space. In this case the transition matrix element is factored into two parts: the envelope-function part and an overlap integral of carrier Bloch functions [Eq. (23)]:

$$\begin{aligned} &|\langle\Psi_{j'\sigma'\mathbf{k}'}|\hat{V}_{\mathrm{int}}|\Psi_{j\sigma\mathbf{k}}\rangle|^2\\ &\quad=|\langle e^{i\mathbf{k}'\cdot\mathbf{r}}|\hat{V}_{\mathrm{int}}|e^{i\mathbf{k}\cdot\mathbf{r}}\rangle|^2 G(j\sigma\mathbf{k}\to j'\sigma'\mathbf{k}'), \end{aligned} \tag{31}$$

where the Bloch overlap factor[45] is defined as

$$G(j\sigma\mathbf{k}\to j'\sigma'\mathbf{k}')=|\langle j'\sigma'\mathbf{k}'|j\sigma\mathbf{k}\rangle|^2. \tag{32}$$

Since the matrix element in Eq. (32) does not vanish identically due to symmetry properties, we neglect small mixture of states with different symmetry in Eq. (24).

The Bloch factor for conduction electrons is given by $G(c\sigma\mathbf{k}\to c\sigma'\mathbf{k}')=\delta_{\sigma,\sigma'}$ and the transition matrix element in Eq. (31) is determined solely by its envelope-function part. In general for holes, the Bloch factor (32) depends on both the initial and the final particle wave vectors and does not vanish for transitions between different valence bands.[45] Thus the Bloch factor (as well as the complicated dispersion law) is mainly responsible for the qualitative difference in electron and hole scattering processes.

For calculation of the Bloch factor in Eq. (32) we use the vector representation of functions $|j\sigma\mathbf{k}\rangle$ in Eq. (25) together with the definitions of bases $|u_i,\sigma\rangle_\varphi$ or $|v_i,\sigma\rangle_\varphi$ in Eqs. (17) and (21). The scalar product of basis functions depends on the difference in polar angles φ and φ' of initial and final wave vectors, i.e.,

$$\begin{aligned} {}_{\varphi'}\langle u_{n'},\sigma'|u_n,\sigma\rangle_\varphi&={}_{\varphi'}\langle v_{n'},\sigma'|v_n,\sigma\rangle_\varphi\\ &=\delta_{n,n'}\mathcal{R}_{n\sigma\sigma'}(\varphi-\varphi'). \end{aligned}$$

Here the rotational function $\mathcal{R}(\varphi)$ is defined as

$$\mathcal{R}_{n\sigma\sigma'}(\varphi)={}_0\langle u_n,\sigma'|u_n,\sigma\rangle_\varphi \tag{33}$$

and is found from Eq. (17) or (21): $\mathcal{R}_{1++}=\mathcal{R}_{1--}=\cos(3\varphi/2)$, $\mathcal{R}_{1+-}=\mathcal{R}_{1-+}=-i\sin(3\varphi/2)$, $\mathcal{R}_{2++}=\mathcal{R}_{2--}=\mathcal{R}_{3++}=\mathcal{R}_{3--}=\cos(\varphi/2)$, and $\mathcal{R}_{2+-}=\mathcal{R}_{2-+}=\mathcal{R}_{3+-}=\mathcal{R}_{3-+}=i\sin(\varphi/2)$. Substituting Eqs. (25) and (33) into Eq. (32), we find the Bloch factor for ''spin''-conserving transitions

$$\begin{aligned} G(j\sigma\mathbf{k}\to j'\sigma\mathbf{k}')=\Big|&u_{j\mathbf{k}\sigma}^{(1)}u_{j'\mathbf{k}'\sigma}^{(1)*}\cos\frac{3\varphi}{2}+(u_{j\mathbf{k}\sigma}^{(2)}u_{j'\mathbf{k}'\sigma}^{(2)*}\\ &+u_{j\mathbf{k}\sigma}^{(3)}u_{j'\mathbf{k}'\sigma}^{(3)*})\cos\frac{\varphi}{2}\Big|^2 \end{aligned} \tag{34}$$

and for scattering with a ''spin'' flip, denoting by a $\overline{\sigma}$ ''spin'' opposite σ,

$$\begin{aligned} G(j\sigma\mathbf{k}\to j'\overline{\sigma}\mathbf{k}')=\Big|&u_{j\mathbf{k}\sigma}^{(1)}u_{j'\mathbf{k}'\overline{\sigma}}^{(1)*}\sin\frac{3\varphi}{2}-(u_{j\mathbf{k}\sigma}^{(2)}u_{j'\mathbf{k}'\overline{\sigma}}^{(2)*}\\ &+u_{j\mathbf{k}\sigma}^{(3)}u_{j'\mathbf{k}'\overline{\sigma}}^{(3)*})\sin\frac{\varphi}{2}\Big|^2, \end{aligned} \tag{34'}$$

where $\varphi=\varphi_{\mathbf{k}}-\varphi_{\mathbf{k}'}$ is the angle between projections of the initial and final wave vectors on the lattice base plane.

Finally, the Bloch factor, averaged on nonpolarized initial and final states, is given by a noncoherent sum of Eqs. (34) and (34′). Neglecting the linear in $\mathbf{k}_\perp$ terms, we obtain

$$
\begin{aligned}
&G(j\mathbf{k}\to j'\mathbf{k}')\\
&\quad\equiv\frac{1}{2}\sum_{\sigma,\sigma'}G(j\sigma\mathbf{k}\to j'\sigma'\mathbf{k}')\\
&\quad=\left|u^{(1)}_{j\mathbf{k}}u^{(1)*}_{j'\mathbf{k}'}\cos\frac{3\varphi}{2}+(u^{(2)}_{j\mathbf{k}}u^{(2)*}_{j'\mathbf{k}'}+u^{(3)}_{j\mathbf{k}}u^{(3)*}_{j'\mathbf{k}'})\cos\frac{\varphi}{2}\right|^2\\
&\qquad+\left|u^{(1)}_{j\mathbf{k}}u^{(1)}_{j'\mathbf{k}'}\sin\frac{3\varphi}{2}-(u^{(2)}_{j\mathbf{k}}u^{(2)}_{j'\mathbf{k}'}+u^{(3)}_{j\mathbf{k}}u^{(3)}_{j'\mathbf{k}'})\sin\frac{\varphi}{2}\right|^2.
\end{aligned}
\tag{35}
$$

To illustrate the use of Eq. (35) for the spin-averaged Bloch factor G, let us consider the limiting case of heavy and light holes in an unstrained *cubic* crystal, neglecting effects of warping. Applying the cubic approximation in Eqs. (8) and (9′) and setting $\Delta_{\rm cr}=0$, we find, from the Hamiltonian in Eq. (2), the normalized eigenvectors of heavy and light holes:

$$
\mathbf{u}_{\mathrm{HH},\mathbf{k}}=\begin{bmatrix}\frac{1}{2}\sin\vartheta-i\cos\vartheta\\ -\frac{\sqrt{3}}{2}\sin\vartheta\\ 0\end{bmatrix},
$$

$$
\mathbf{u}_{\mathrm{LH},\mathbf{k}}=\frac{1}{\sqrt{1+3\cos^2\vartheta}}\begin{bmatrix}\frac{\sqrt{3}}{2}(\sin^2\vartheta-i\sin2\vartheta)\\ \frac{1}{2}(1+3\cos^2\vartheta)\\ 0\end{bmatrix},
$$

where $\vartheta=\vartheta_{\mathbf{k}}$ is the angle between the wave vector $\mathbf{k}$ and the c axis.

Substituting $\mathbf{u}_{j\mathbf{k}}$ into Eq. (35), we recover the standard expressions for Bloch factors in cubic materials,[44] which depend exclusively on the angle α between vectors $\mathbf{k}$ and $\mathbf{k}'$:

$$
\begin{aligned}
&G(\mathrm{HH}\to\mathrm{HH})=G(\mathrm{LH}\to\mathrm{LH})=\frac{1}{4}(1+3\cos^2\alpha),\\
&G(\mathrm{HH}\to\mathrm{LH})=\frac{3}{4}\sin^2\alpha.
\end{aligned}
\tag{36}
$$

B. Optical transitions: Valence to conduction bands

Consider the carrier interaction with an electromagnetic wave specified by vector potential $\mathbf{A}$. For the plane wave with mometum $\boldsymbol{\kappa}$ and frequency ω the complex vector potential has the form $\mathbf{A}(\mathbf{r},t)=\mathbf{e}A_0\exp(i\boldsymbol{\kappa}\cdot\mathbf{r}-i\omega t)$, where $\mathbf{e}$ is a unit vector in the direction of vector potential $\mathbf{A}$ and electric field $\mathbf{E}=(i\omega/c)\mathbf{A}$.

Applying the Coulomb gauge for the vector potential $\nabla\cdot\mathbf{A}=0$, the perturbation (to carrier Hamiltonian) due to interaction with the electromagnetic wave can be written as

$$
\hat{V}_{\rm int}=\frac{e}{m_0c}\left(\mathbf{A}\cdot\hat{\mathbf{p}}+\frac{e}{2c}A^2\right),
\tag{37}
$$

where $\hat{\mathbf{p}}=-i\hbar\nabla$ is the momentum operator. The interaction due to the second term in Eq. (37) is forbidden in many cases because of selection rules; otherwise it can be neglected for sufficiently small field intensity.

The time-independent matrix element for one photon-assisted transition between the initial state $\Psi_{j\sigma\mathbf{k}}$ and the final state $\Psi_{j'\sigma'\mathbf{k}'}$ is written, using Eqs. (23) and (37), as

$$
\begin{aligned}
&\langle\Psi_{j'\sigma'\mathbf{k}'}|\hat{V}_{\rm int}|\Psi_{j\sigma\mathbf{k}}\rangle\\
&\quad=\delta_{\mathbf{k}',\mathbf{k}+\boldsymbol{\kappa}}\frac{eA_0}{m_0c}\int d^3rU^*_{j'\sigma'\mathbf{k}+\boldsymbol{\kappa}}[\mathbf{e}\cdot\hat{\mathbf{p}}+\hbar\mathbf{k}\cdot\mathbf{e}]U_{j\sigma\mathbf{k}}.
\end{aligned}
\tag{38}
$$

Below we use the *dipole approximation*, neglecting a small photon wave vector, $\boldsymbol{\kappa}\approx\mathbf{0}$. In this case the contribution of the second term in square brackets in Eq. (38) vanishes for transitions between different bands[46] due to orthogonality of corresponding Bloch functions U. In this case the matrix element in Eq. (38) is proportional to

$$
M_{j\sigma\to j'\sigma'}(\mathbf{k})\equiv\int d^3rU^*_{j'\sigma'\mathbf{k}}\mathbf{e}\cdot\hat{\mathbf{p}}\;U_{j\sigma\mathbf{k}}.
\tag{39}
$$

Below we calculate the matrix element in Eq. (39) for dipole optical transitions between conduction and valence bands. The initial electron state belongs to a valence band j, where j denotes a HH, LH, or SH, and is characterized by a ''spin'' σ_v. The final state, corresponding to the conduction band c and spin σ_c, is described by an orbital Bloch function $\langle S|$ and spinor $\langle\sigma_c|=\langle\uparrow|,\langle\downarrow|$, corresponding to two directions of electron spin 1/2. With the help of Eq. (24) one can rewrite Eq. (39) as

$$
M_{j\sigma_v\to c\sigma_c}(\mathbf{k})=\langle S|\langle\sigma_c|\mathbf{e}\cdot\hat{\mathbf{p}}|j\sigma_v\mathbf{k}\rangle.
\tag{40}
$$

Here we neglect the small contributions to the Bloch functions in Eq. (24) with symmetry properties different from the Γ point.

Using a vector representation of the Bloch function in Eq. (25), we find

$$
\begin{aligned}
M_{j\sigma_v\to c\sigma_c}&=\sum_{i=1}^{3}u^{(i)}_{j\mathbf{k}}\langle S|\langle\sigma_c|\mathbf{e}\cdot\hat{\mathbf{p}}|u_i,\sigma_v\rangle\\
&=\sum_{i=1}^{3}v^{(i)}_{j\mathbf{k}}\langle S|\langle\sigma_c|\mathbf{e}\cdot\hat{\mathbf{p}}|v_i,\sigma_v\rangle.
\end{aligned}
\tag{41}
$$

For simplicity we drop the spin index σ_v from coordinates of the Bloch vector $\mathbf{u}_{j\mathbf{k}\sigma_v}$.

Since the interaction Hamiltonian in Eq. (37) is diagonal in carrier spin, it is convenient to first calculate the matrix elements of momentum operator $\hat{\mathbf{p}}$ in the valence-band basis $|v_i,\sigma\rangle$. Because of symmetry properties of the Bloch functions, the only nonzero matrix elements between the basis functions are given by (cf. Appendix C)

$$
\langle S|\hat{p}_z|1,0\rangle=P_z,\quad\langle S|\hat{p}_+|1,-1\rangle=-\langle S|\hat{p}_-|1,1\rangle=\sqrt{2}P_\perp,
\tag{42}
$$

TABLE I. Matrix elements $\langle S|\langle\sigma_c|\mathbf{e}\cdot\hat{\mathbf{p}}|v_i,\sigma_v\rangle$, of optical transitions between conduction-band states and valence-band basis states in Eq. (21).

$\mathbf{e}\cdot\hat{\mathbf{p}}$	$\lvert v_1,\pm\rangle$	$\lvert v_2,\pm\rangle$	$\lvert v_3,\pm\rangle$
$\langle S\lvert\langle\uparrow\rvert$	$-\frac{1}{2}P_\perp e^{i\varphi}\sin\vartheta$	$-\frac{1}{2}P_\perp e^{-i\varphi}\sin\vartheta$	$\mp\frac{i}{\sqrt{2}}P_z\cos\vartheta$
$\langle S\lvert\langle\downarrow\rvert$	$\mp\frac{i}{2}P_\perp e^{-i\varphi}\sin\vartheta$	$\mp\frac{i}{2}P_\perp e^{i\varphi}\sin\vartheta$	$\frac{1}{\sqrt{2}}P_z\cos\vartheta$

where $\hat{p}_\pm=\hat{p}_x\pm i\hat{p}_y$; two momentum matrix element constants can be defined as $P_z\equiv\langle S|\hat{p}_z|Z\rangle$ and $P_\perp\equiv\langle S|\hat{p}_x|X\rangle$.

Due to cylindrical symmetry, the matrix element (40) depends only on the difference $\varphi\equiv\varphi_{\mathbf{E}}-\varphi_{\mathbf{k}}$ between base-plane-projected angles of vectors $\mathbf{e}\|\mathbf{E}$ and $\mathbf{k}$. To simplify calculations, we choose $\varphi_{\mathbf{k}}=0$ and denote the spherical angles of vector $\mathbf{e}$ by φ and ϑ, i.e., $\mathbf{e}=(\sin\vartheta\cos\varphi,\sin\vartheta\sin\varphi,\cos\vartheta)$. Applying Eq. (42) and the identity

$$\mathbf{e}\cdot\hat{\mathbf{p}}=\frac{1}{2}\sin\vartheta(e^{i\varphi}\hat{p}_-+e^{-i\varphi}\hat{p}_+)+\hat{p}_z\cos\vartheta,$$

we obtain the matrix elements of the operator $\mathbf{e}\cdot\hat{\mathbf{p}}$ between conduction-band states and the non-relativistic-like basis set $|v_i,\sigma_v\rangle$ listed in Table I. Using Eq. (20) to transform the set $|v_i,\sigma_v\rangle$ to the cubiclike Bloch functions basis $|u_i,\sigma_v\rangle$, we also obtain the matrix elements $\langle S|\langle\sigma_c|\mathbf{e}\cdot\hat{\mathbf{p}}|u_i\sigma_v\mathbf{k}\rangle$ shown in Table II. Finally, one can define[47] the squared total matrix element as a noncoherent sum of $|M|^2$ over four possible sets of spin configurations:

$$|M^{\rm tot}_{j\to c}|^2=\sum_{\sigma_c,\sigma_v}|M_{j\sigma_v\to c\sigma_c}|^2. \tag{43}$$

Consider the special case of a hole wave vector parallel to the c axis, i.e., $k_\perp=0$. In this situation the angle $\varphi_{\mathbf{k}}$ is indeterminate and one can set $\varphi=0$ in Table I. Substituting Eqs. (26), (29), and (41) into Eq. (43), we find

$$|M^{\rm tot}_{\rm HH\to c}|^2=|P_\perp|^2\sin^2\vartheta,$$

$$\left.\begin{matrix}|M^{\rm tot}_{\rm LH\to c}|^2\\ |M^{\rm tot}_{\rm SH\to c}|^2\end{matrix}\right\}=|P_\perp|^2\sin^2\vartheta\left\{\begin{matrix}\cos^2\phi\\ \sin^2\phi\end{matrix}\right\}+2|P_z|^2\cos^2\vartheta\left\{\begin{matrix}\sin^2\phi\\ \cos^2\phi\end{matrix}\right\}, \tag{44}$$

where $\phi=\phi^{(v)}_{\rm LH}$ is given by Eq. (30).

In the limit of unstrained wurtzite crystals at $\mathbf{k}=\mathbf{0}$, we obtain $\sin^2\phi=E^{(0)}_{\rm LH}/(E^{(0)}_{\rm LH}-E^{(0)}_{\rm SH})$, and Eq. (43) is reduced to the well-known expression for transitions from the valence-band edges.[19] Furthermore, for *cubic* crystals $|P_z|=|P_\perp|\to|P|$ and $\sin^2\phi=2/3$, so that Eq. (43) reproduces the results for optical transitions in cubic materials.[47]

The absolute values of constants $|P_{z,\perp}|^2$ can be estimated from experimentally measured conduction-band effective masses $m^{(c)}_{z,\perp}$ using the result of $\mathbf{k}\cdot\mathbf{p}$ theory:

$$\frac{m_0}{m^{(c)}_{z,x}}=1+\frac{2}{m_0}\sum_{j\neq c}\frac{|\langle c|\hat{p}_{z,x}|j\rangle|^2}{E^{(0)}_c-E^{(0)}_j}. \tag{45}$$

Neglecting the contribution to $m^{(c)}$ from all bands j except the three top valence bands (this is a less accurate approximation for GaN than for GaAs) and instead using the gap value E_g for all energy differences in Eq. (45), we find the estimation for constants $P_{z,\perp}$,

$$\frac{2|P_{z,\perp}|^2}{m_0}\simeq E_g\left(\frac{m_0}{m^{(c)}_{z,\perp}}-1\right). \tag{46}$$

C. Inter-valence-band optical transitions

In this subsection we calculate the one-photon-assisted matrix element for transitions within valence bands j,j', which denote the HH, LH, and SH, using the dipole approximation in Eq. (40). In this case it is not possible to substitute the exact Bloch functions in Eq. (24), $U_{j\sigma\mathbf{k}}$, by their component with Γ-point symmetry properties, $|j\sigma\mathbf{k}\rangle$. Unlike for the transitions between the valence and conduction band in Sec. IV B, the Bloch function contributions of zeroth order in k vanish due to symmetry properties (except the small part proportional to the spin splitting constant k_s).

However, for intervalence-band transitions both the initial and final states are described by the envelope-function Hamiltonian H, and one can use the following expressions[48,49] for the momentum matrix element:

$$\begin{aligned}\langle U_{j'\sigma'\mathbf{k}'}|\hat{\mathbf{p}}|U_{j\sigma\mathbf{k}}\rangle&=\frac{m_0}{\hbar}\langle U_{j\sigma\mathbf{k}}\left|\frac{\partial\mathcal{H}}{\partial\mathbf{k}}\right|U_{j\sigma\mathbf{k}}\rangle\\&=\frac{m_0}{\hbar}{}_0\langle j'\sigma'\mathbf{k}\left|\overline{\frac{\partial H}{\partial\mathbf{k}}}\right|j\sigma\mathbf{k}\rangle_0+O(k).\end{aligned} \tag{47}$$

The operator identity $\hat{\mathbf{p}}=(im_0/\hbar)[\mathcal{H}\mathbf{r}-\mathbf{r}\mathcal{H}]=(m_0/\hbar)\partial\mathcal{H}/\partial\mathbf{k}$ was used in the first line of Eq. (47), where $\mathcal{H}$ is a

TABLE II. Matrix elements $\langle S|\langle\sigma_c|\mathbf{e}\cdot\hat{\mathbf{p}}|u_i,\sigma_u\rangle$ of optical transitions between conduction-band states and valence-band basis states in Eq. (17).

$\mathbf{e}\cdot\hat{\mathbf{p}}$	$\lvert u_1,\pm\rangle$	$\lvert u_2,\pm\rangle$	$\lvert u_3,\pm\rangle$
$\langle S\lvert\langle\uparrow\rvert$	$-\frac{1}{2}P_\perp e^{i\varphi}\sin\vartheta$	$-\frac{\sqrt{3}}{6}[P_\perp e^{-i\varphi}\sin\vartheta\mp 2iP_z\cos\vartheta]$	$-\frac{1}{\sqrt{6}}[P_\perp e^{-i\varphi}\sin\vartheta\pm iP_z\cos\vartheta]$
$\langle S\lvert\langle\downarrow\rvert$	$\mp\frac{i}{2}P_\perp e^{-i\varphi}\sin\vartheta$	$\frac{\sqrt{3}}{6}[\mp iP_\perp e^{i\varphi}\sin\vartheta-2P_z\cos\vartheta]$	$\frac{1}{\sqrt{6}}[\mp iP_\perp e^{i\varphi}\sin\vartheta+P_z\cos\vartheta]$

full electron Hamiltonian. Replacement of the exact Hamiltonian $\mathcal{H}$ by its envelope-function counterpart H was justified by Szmulowicz[49] using the unitary transformation of Bloch functions basis and diagonalizing the contribution of the Γ-like part of $\mathcal{H}$. Hamiltonian H in Eq. (47) is not block diagonal since it is defined with the fixed basis set $|j\sigma\mathbf{k}\rangle_0$ corresponding to $\varphi=0$.

The transfer to the block-diagonal form of the Hamiltonian H is achieved using relations $|j\sigma\mathbf{k}\rangle_\varphi = U_\varphi |j\sigma\mathbf{k}\rangle_0$ and $H = U_\varphi H U_{-\varphi}$, where U_φ is a 6×6 unitary transformation matrix specified by Eq. (17) or (21). Substituting the Bloch function representation of Eq. (25) into Eq. (47), we find the matrix element for optical transitions from Eq. (39),

$$\begin{aligned} M_{j\sigma\to j'\sigma'}(\mathbf{k}) &= -\hbar \sum_{i,i'=1}^{3} \{\delta_{\sigma',\sigma}[K^{(z)}_{\sigma,i'i}\cos\vartheta + K^{(\perp)}_{\sigma,i'i}\sin\vartheta\cos\varphi] \\ &\quad + K^{(\varphi)}_{\sigma'\sigma,i'i}\sin\vartheta\sin\varphi\} v^{(i')*}_{j'\mathbf{k}\sigma'} v^{(i)}_{j\mathbf{k}\sigma}. \end{aligned} \tag{48}$$

Here $\varphi=\varphi_{\mathbf{E}}-\varphi_{\mathbf{k}}$, where $\varphi_{\mathbf{E}}$ and $\vartheta=\vartheta_{\mathbf{E}}$ are spherical angles of the polarization vector $\mathbf{e}\|\mathbf{E}$. Matrices K have dimensions of a wave vector and are defined as

$$K^{(z,\perp)}_{\pm} = -\frac{m_0}{\hbar^2}\frac{\partial H_{\pm}}{\partial k_{z,\perp}}, \quad K^{(\varphi)} = -\frac{m_0}{\hbar^2 k_\perp}\left[H, \frac{dU_\varphi}{d\varphi}U_{-\varphi}\right]. \tag{49}$$

Using the explicit Hamiltonian form $H_{\pm}$ in Eq. (22), we obtain

$$K^{(z)} = \begin{bmatrix} (\gamma_{1z}-2\gamma_{3z})k_z & 0 & \pm i\frac{3}{\sqrt{2}}\overline{\gamma_z}k_\perp \\ 0 & (\gamma_{1z}-2\gamma_{3z})k_z & \pm i\frac{3}{\sqrt{2}}\overline{\gamma_z}k_\perp \\ \mp i\frac{3}{\sqrt{2}}\overline{\gamma_z}k_\perp & \mp i\frac{3}{\sqrt{2}}\overline{\gamma_z}k_\perp & (\gamma_{1z}+4\gamma_{3z})k_z \end{bmatrix}$$

and

$$K^{(\perp)} = \begin{bmatrix} (\gamma_{1\perp}+\gamma_{3\perp})k_\perp & 3\overline{\gamma_\perp}k_\perp & \mp k_s \pm i\frac{3}{\sqrt{2}}\overline{\gamma_z}k_z \\ 3\overline{\gamma_\perp}k_\perp & (\gamma_{1\perp}+\gamma_{3\perp})k_\perp & \mp k_s \pm i\frac{3}{\sqrt{2}}\overline{\gamma_z}k_z \\ \mp k_s \mp i\frac{3}{\sqrt{2}}\overline{\gamma_z}k_z & \mp k_s \mp i\frac{3}{\sqrt{2}}\overline{\gamma_z}k_z & (\gamma_{1\perp}-2\gamma_{3\perp})k_\perp \end{bmatrix}.$$

Thus Eq. (48) expresses the matrix elements for optical transitions between valence bands in terms of Bloch vector components $v_{j\mathbf{k}}$ of initial and final hole states. The total square matrix element is given by noncoherent sum over different spin configurations

$$|M^{\mathrm{tot}}_{j\to j'}|^2 = \sum_{\sigma,\sigma'} |M_{j\sigma\to j\sigma'}|^2. \tag{50}$$

To illustrate the derived expressions, we consider the particular case of a hole wave vector parallel to the c axis, i.e., $k_\perp=0$. Substituting Eqs. (26), (29), and (41) into Eqs. (48) and (50), we find the total squared matrix element for optical transitions between different valence bands:

$$\begin{aligned} \left.\begin{matrix} |M^{\mathrm{tot}}_{\mathrm{LH}\to\mathrm{HH}}|^2/\hbar^2 \\ |M^{\mathrm{tot}}_{\mathrm{SH}\to\mathrm{HH}}|^2/\hbar^2 \end{matrix}\right\} &= (9\overline{\gamma_z^2}k_z^2 + 2k_s^2)\left\{\begin{matrix}\sin^2\phi \\ \cos^2\phi\end{matrix}\right\}\sin^2\vartheta, \\ |M^{\mathrm{tot}}_{\mathrm{SH}\to\mathrm{LH}}|^2/\hbar^2 &= (9\overline{\gamma_z^2}k_z^2 + 2k_s^2\cos^2 2\phi)\sin^2\vartheta \\ &\quad + 18\gamma_{3z}^2 k_z^2 \sin^2 2\phi\cos^2\vartheta. \end{aligned} \tag{51}$$

Here $\phi=\phi^{(v)}_{\mathrm{LH}}$ is given by Eq. (30).

As seen from Eq. (51), at $\mathbf{k}=\mathbf{0}$ the transition matrix elements do not vanish identically as in cubic crystals, but are proportional to parameter k_s. The finite value of the spin-splitting constant k_s and violation of cubiclike selection rules for intervalence-band optical transitions are directly related to the absence of a horizontal reflection plane in the wurtzite point group C_{6v} (cf. Appendix C).

V. MATERIAL PARAMETERS AND NUMERICAL RESULTS

Despite a number of experimental results for group-III nitride material properties, difficulties in fabrication of unstrained and sufficiently pure samples prohibit formulating a reliable and consistent set of experimental material parameters. At present, the conduction- and valence-band parameters, as well as deformation potential constants, are obtained from a comparison of experimental data with results of *ab initio* calculations.

In Table III we present several sets of Luttinger-like parameters γ and splitting energies Δ for bulk GaN and AlN. In the following calculations we use the material parameters of GaN from the first line of the Table III. Luttinger-like parameters are obtained using Eq. (A1) from the results of *ab initio* calculations by Suzuki *et al.*,[31] with the missing parameter γ_{2z} or A_6 estimated from the quasicubic approximation in Eq. (9) or (B6).[51] Constant k_s, responsible for the removal of spin degeneracy, is neglected in the following calculations.

TABLE III. Valence-band parameters set for wurtzite GaN and AlN. Dimensionless Luttinger-like parameters are calculated from data presented in Ref. 31 (the data of Ref. 35 are listed in parentheses). Splitting energies $\Delta_{1,2,3}$ (in meV) are derived from the experimental data presented in Ref. 50.

	γ_{1z}	$\gamma_{1\perp}$	γ_{2z}	$\gamma_{2\perp}$	γ_{3z}	$\gamma_{3\perp}$	Δ_1	$\Delta_2 \approx \Delta_3$
GaN	2.47	2.85	$\approx\gamma_{2\perp}$	1.29	0.95	0.95	12.5	5.95
	(2.57)	(2.66)		(1.0)	(0.95)	(0.97)	19.1[a], 72.9[b]	7.0[a], 5.2[b]
AlN	1.54	1.50	$\approx\gamma_{2\perp}$	0.78	0.63	0.62	-215[a], -58.5[b]	6.3[a], 6.8[b]

[a]Reference 16.
[b]Reference 31.

Splitting energies $\Delta_{1,2,3}$ and the deformation potential b are derived from the experimental data of Gil *et al.*[50] on transition energies of A, B, and C excitons versus in-plane biaxial residual strain in the hexagonal GaN epilayers. In our calculations we use Eqs. (14) and (28) together with the most recent experimental values of elasic constants[52] $C_{33}=398$ GPa and $C_{13}=106$ GPa. Nonlinear fitting to strain-dependent transition energies $E_c(0)-E_j(0)$ [see also Fig. 3(b)] results in the following values of splitting energies: $\Delta_1\approx 12.5$ meV, $\Delta_2\approx 5.95$ meV, and $\Delta_3\approx 5.94$ meV, and, within the spherical cubic approximation, a shear deformation potential value of $b\approx -1.67$ eV. These values, deduced from the experimental data,[50] are consistent with the first-principles calculations by Kim *et al.*;[16] deformation potentials δ can be approximated using Eq. (10′). Finally, the valence-band hydrostatic deformation potential a_v is estimated from its gap value $a_g=a_c-a_v\approx -8.16$ eV,[50] using the empirical relation[43] $a_v\approx -a_g/3$.

Figure 3 demonstrates the effect of the in-plane biaxial strain, specified by Eqs. (13) and (14), on hole eigenfunctions and spectra in GaN at $\mathbf{k}=\mathbf{0}$. In Fig. 3(b) we plot the strain-induced change of the valence-band positions (relative to the edge of the conduction band) calculated using Eq. (28); Fig. 3(b) shows the angle ϕ between the Bloch vectors of light holes in cubic and wurtzite crystals [cf. Fig. 2(b)], given by Eqs. (27) and (30). For convenience, we choose the top of the heavy-hole band in unstrained material as the energy reference.

In absence of deformation $\varepsilon=0$, the heavy- and light-hole levels are split due to the hexagonal crystal field (vertical solid line in Fig. 3). Consider now the tensile biaxial strain (dotted vertical line) with components $\varepsilon_{xx}=\varepsilon_{yy}=0.16\%$ and $\varepsilon_{zz}=-0.085\%$, specified by the negative of $\varepsilon^{\mathrm{add}}$ in Eq. (15). As discussed in Sec. II D, the effect of the finite hexagonal crystal splitting term Δ_{cr} can be substituted by the compressive ''internal'' deformation in Eq. (15), corresponding to an additional compressive biaxial strain $\varepsilon^{\mathrm{add}}$. Applying the tensile deformation $-\varepsilon^{\mathrm{add}}$ effectively cancels the contribution Δ_{cr} of the hexagonal component of the crystal field. Thus the valence-band eigenstates and spectrum in wurtzites become similar to those in cubic crystals: hole Bloch functions coincide with their cubic counterparts [i.e., $\phi=0$ in Fig. 3(a)], and degeneracy between heavy- and light-hole bands at the Γ point is restored.

The dashed vertical line in Fig. 3 corresponds to -0.24% compressive strain in GaN lattice matched to the $Al_{0.1}Ga_{0.9}N$ alloy. As the magnitude of the compressive strain is increased, the Bloch vector angle approaches its nonrelativistic limit of $\phi\approx 55°$ (see Sec. III C) and the split-off hole band is further separated from the rest of the bands, while the distance between the heavy- and light-hole bands saturates at the value of $E_{\mathrm{HH}}(0)-E_{\mathrm{LH}}(0)\to(\Delta_1+3\Delta_2)/2\approx 15.2$ meV.

Figure 4 presents the valence-band spectrum of unstrained (solid) and strained (dashed) GaN for wave vector $\mathbf{k}$ being parallel (left) or perpendicular (right) to the crystal c axis. Strain parameters in Fig. 4 correspond to the vertical dashed line in Fig. 3. As seen from Fig. 4, even in unstrained wurtzite material, the valence-band dispersion relations are highly anisotropic and are characterized by an ''anticrossing'' behavior due to a strong mixing of different hole bands. Applying -0.24% compressive strain leads to some quantitative changes in spectrum, while leaving the overall form of the dispersion curves intact. The absence of any profound effect of biaxial strain on the valence-band spectrum can be

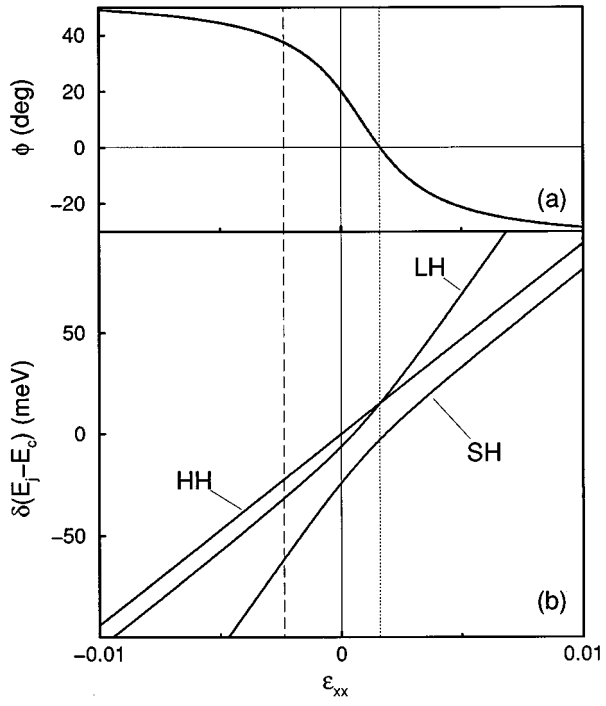

FIG. 3. Effect of biaxial strain ε on eigenfunctions and eigenenergies of heavy, light, and split-off holes at $\mathbf{k}=\mathbf{0}$. (a) Angle $\phi=\phi_{\mathrm{LH}}^{(u)}$ between the Bloch vector of the light holes and axis u_1 in Fig. 2 vs the strain component $\varepsilon_{xx}=\varepsilon_{\perp}/2$. (b) Change in distance between conduction and valence bands, $\delta(E_c-E_j)$, due to biaxial strain.

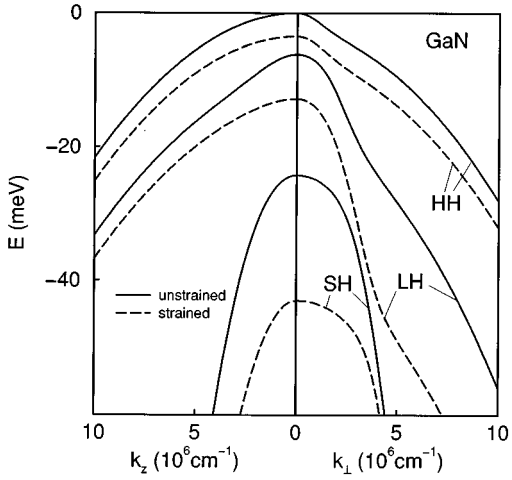

FIG. 4. Dispersion law of holes in unstrained (solid) and strained (dashed) bulk GaN for different directions of the wave vector. Biaxial strain with $\varepsilon_{xx}=-0.242\%$ corresponds to GaN lattice matched to $Al_xGa_{1-x}N$ with $x=0.1$.

understood with the help of Fig. 3: even in the absence of external strain (solid vertical line), wurtzite crystals are already prestrained due to an effective internal deformation. Therefore, finite external deformation in wurtzite structures does not lead to qualitative changes in the hole spectrum or eigenstates, in contrast to the drastic effect of deformation on the degenerate Γ_8 level in cubic crystals.

In Fig. 5 we plot the Bloch overlap factors, calculated from Eq. (35), for elastic hole scattering between different valence bands versus the angle ϑ between initial wave vector $\mathbf{k}$ and the c axis. The wave vector of the final state $\mathbf{k}'$ is chosen so that, despite the change in the direction of $\mathbf{k}$, initial and final wave vectors remain orthogonal to each other. In the limiting case of an unstrained cubic crystal, described by a spherical approximation to the 4×4 Luttinger-Kohn Hamiltonian, substituting $\alpha=\pi/2$ into Eq. (36) would lead to expressions, independent of ϑ: $G(\mathrm{HH}\rightarrow\mathrm{HH})=G(\mathrm{LH}\rightarrow\mathrm{LH})=1/4$ and $G(\mathrm{HH}\rightarrow\mathrm{LH})=3/4$. As seen from Fig. 5, in wurtzite crystals the Bloch overlap factors depend not only on the angle between $\mathbf{k}$ and $\mathbf{k}'$, but also on the directions of the initial and final wave vectors. The value of the Bloch overlap factor, given by Eq. (35), is needed for the calculation of hole scattering rates by Coulomb impurities, polar optical phonons, and charged carriers.

In Figs. 6 and 7 we present the dimensionless total square matrix elements for the optical transition of a hole with a wave vector parallel to the c axis (i.e., $k_\perp=0$). Matrix elements for transitions from valence to conduction bands (Fig. 6) are calculated using Eq. (44), while those for intervalence-band transitions (Fig. 7) are obtained with the help of Eq. (51). The cubic approximation $P_z=P_\perp$ is used for the momentum matrix element constants. Figures 6(a) and 7(a) show the polarization dependence of the optical transitions in unstrained (solid) and strained (dashed) wurtzite GaN. In agreement with Eq. (44), the matrix elements of optical transitions from any valence band to the conduction band are equal (and independent of strain) at the polarization angle $\vartheta=\arctan\sqrt{2}\approx55°$.

In Figs. 6(b) and 7(b) we plotted the dependence of the

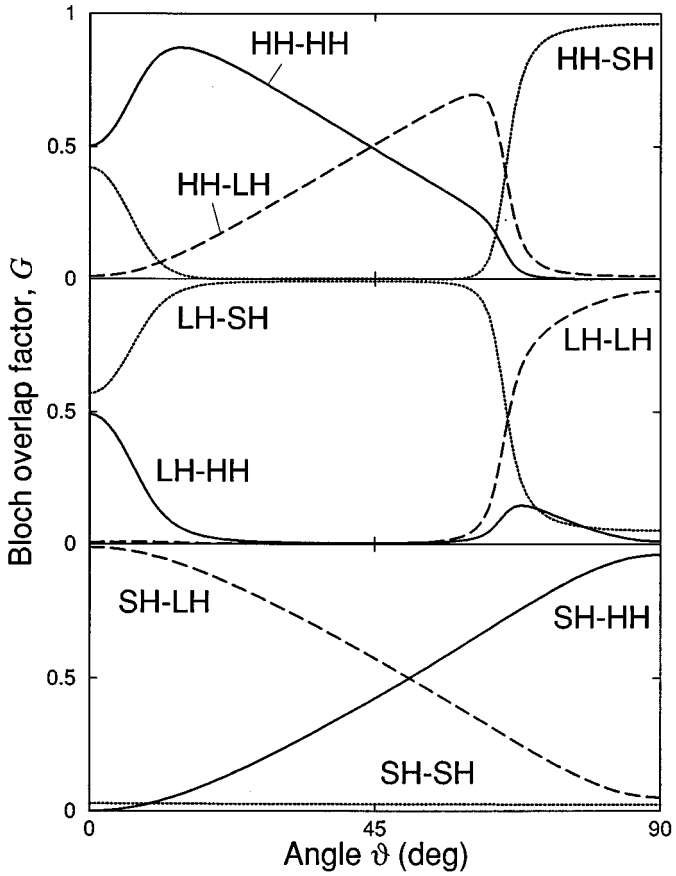

FIG. 5. Bloch overlap factors $G(j\mathbf{k}\rightarrow j'\mathbf{k}')$ for elastic hole scattering between bands j,j', which denote the HH, LH, and SH. The hole energy is taken at 100 meV below level Γ_9. The wave vector of the initial state $\mathbf{k}$ is specified by spherical angles $\varphi=0$ and $0<\vartheta<\pi/2$; for the final state the angles $\varphi'=\vartheta'=\pi/2$ are chosen.

optical transition matrix elements on the in-plane biaxial strain for the wave polarization parallel (solid) and perpendicular (dashed) to the c axis. As follows from Eqs. (44) and (51), the magnitude of $M^{\mathrm{tot}}_{\mathrm{HH}\rightarrow c}$ is not changed with strain. The strain dependence for other transitions is specified by the angle $\phi=\phi^{(v)}_{\mathrm{LH}}$ given by Eq. (30). The dotted vertical line in Figs. 6(b) and 7(b) marks the intersection of several curves and corresponds to the condition $\sin^2\phi=\cos^2\phi$ satisfied at $\phi=-\pi/4$. Finally, we notice that the absolute magnitudes of transition rates for the processes under consideration are proportional to the energy parameters $2|P|^2/m_0$ and $\hbar^2k_z^2/2m_0$. Using Eq. (46), numerical values[1] $m^{(c)}=0.19m_0$ and $E_g=3.4$ eV, and approximating the hole energy by the thermal energy at $T=300$ K, we obtain the following estimates: $2|P|^2/m_0\sim15$ eV and $\hbar^2k_z^2/2m_0\sim25$ meV. Thus the intensity of the valence-band to conduction-band optical transitions is substantially higher than the intensity of intervalence-band optical transitions, since the latter are forbidden (to the lowest order in k) due to the selection rules.

VI. CONCLUSION

In this paper we have addressed several issues dealing with the description of hole energy spectra and transitions in wide-band-gap wurtzite materials within the envelope-

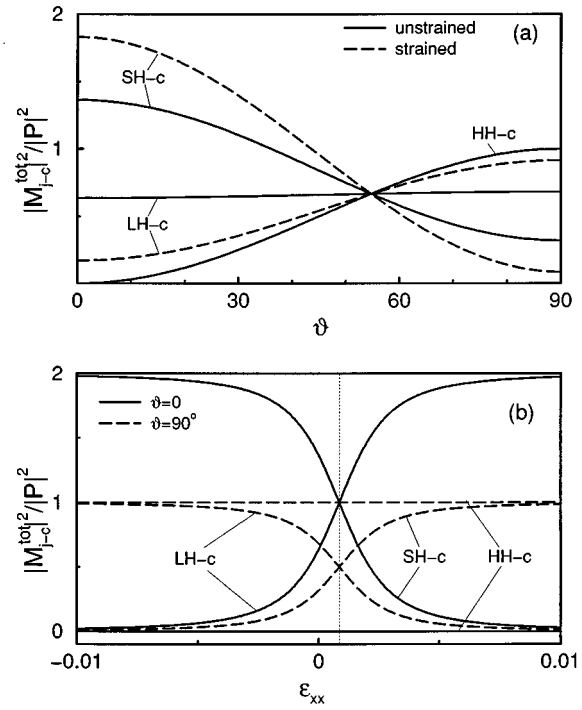

FIG. 6. Matrix element of optical transitions between valence and conduction bands, $|M^{\mathrm{tot}}_{j\to c}|^2/|P|^2$, for unstrained (solid) and strained (dashed) bulk GaN at $\mathbf{k}=\mathbf{0}$. The biaxial strain is the same as in Fig. 4. (a) Dependence on the angle ϑ between the light polarization vector and the c axis. (b) Dependence on biaxial strain.

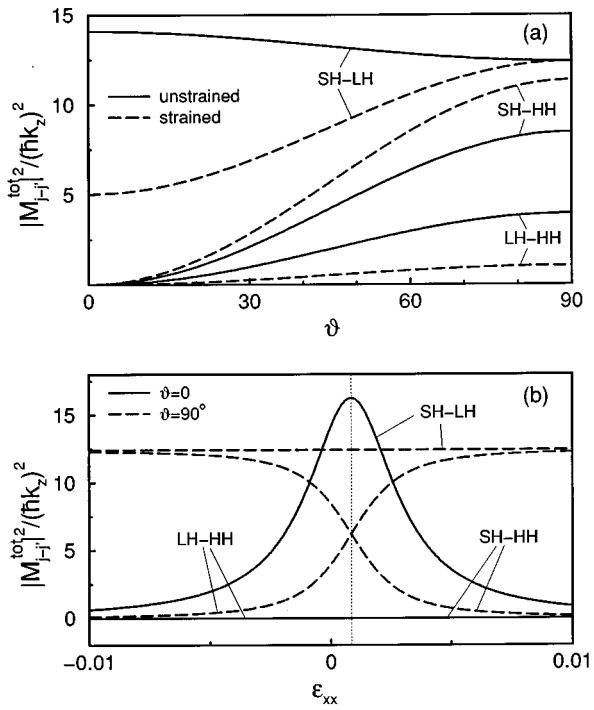

FIG. 7. Matrix element of optical transitions between valence bands, $|M^{\mathrm{tot}}_{j\to j'}|^2/\hbar^2k_z^2$ for bulk GaN and $k_\perp=0$. The rest of the notations coincide with those in Fig. 6.

function formalism. We have corrected the frequently used quasicubic approximation for the wurtzite band-curvature parameters and deformation potential constants. The analogy between cubic and wurtzite valence-band Hamiltonians was elucidated by reformulating the latter in terms of Luttinger-like parameters γ and establishing the connection, in Eq. (12), between the hexagonal crystal splitting energy and additional, ''built-in'' strain in wurtzites.

In view of the importance of block diagonalization of the full Hamiltonian for efficient band-structure and transition rate calculations, we have established a correspondence between different proposed forms of 3×3 blocks and discussed their physical meanings. We demonstrated that these forms correspond to different coordinate frames in the three-dimensional Bloch space that can be transformed into one another by means of a rotation around the heavy-hole axis (see Fig. 2).

Finally, using a uniform approach based on block-diagonal forms of wurtzite Hamiltonian, we derived matrix elements for various transition processes involving valence-band carriers: scattering of holes, optical transitions from the valence band to the conduction band, and infrared transitions between the valence bands. Special attention was taken for reproducing the corresponding results for cubic symmetry (with warping neglected) as a special case of the wurtzite parameter set. The numerical calculation of the transition matrix elements has been performed using a set of material constants of GaN.

ACKNOWLEDGMENTS

The authors acknowledge many helpful discussions with Dr. J. M. Zavada. We are grateful to Kwiseon Kim and her coauthors in Ref. 16 for making their results available to us prior to publication. This study was supported by the U.S. Army Research Office and the Office of Naval Research.

APPENDIX A: COMPARISON OF NOTATIONS

Relations between different notations for valence-band reciprocal mass parameters (γ_i, etc.) and deformation potentials (D_i, etc.) in cubic materials are listed in Table IV (expressions in the same line are equal). For simplicity, we set $\hbar^2/2m_0\to1$. The parameter C of Refs. 21 and 53 is related to parameters in Table IV by $C^2=D^2-3B^2$. Reciprocal mass parameters and deformation potential constants of the same vertical row in Table IV are related to each other according to Eq. (6).

In wurtzite materials, the Luttinger-like parameters γ, in-

TABLE IV. Comparison of notations for the band curvature and strain parameters in the valence bands of cubic materials.

Ref. 22	Refs. 21,53, and 19	Ref. 53	Ref. 54
γ_1	$-A$	$-(L+2M)/3$	$-r_1/\sqrt{3}$
γ_2	$-B/2$	$(M-L)/6$	$-r_3/2\sqrt{3}$
γ_3	$-D/2\sqrt{3}$	$-N/6$	$-r_5/2\sqrt{6}$
Ref. 55	Ref. 19	Ref. 19	Ref. 54
$-D_d^v$	$-a_v$	$-(l+2m)/3$	$-d_1/\sqrt{3}$
$D_u/3$	$-b/2$	$(m-l)/6$	$-d_3/2\sqrt{3}$
$D_u'/3$	$-d/2\sqrt{3}$	$-n/6$	$-d_5/2\sqrt{6}$

troduced in this paper, are related to parameters A of Bir and Pikus[19] in the following way:

$$\gamma_{1z}=-A_1-2A_3/3,\quad \gamma_{2z}=A_6/\sqrt{8}-A_3/12,\quad \gamma_{3z}=A_3/6,$$
$$\gamma_{1\perp}=-A_2-2A_4/3,\quad \gamma_{2\perp}=2A_4/3+A_5,\quad \gamma_{3\perp}=-A_4/3. \tag{A1}$$

The relation between deformation potentals can be obtained from the above formulas by changing A to D and γ to δ.

APPENDIX B: TRANSFORMATION OF THE CUBIC HAMILTONIAN

Below we outline the derivation of the quasicubic approximation for wurtzite crystals and correct a mistake[38] in Ref. 19. We transform the cubic Hamiltonian in Eq. (2) to a new coordinate frame with basis vectors $\mathbf{e}'_x$, $\mathbf{e}'_y$, and $\mathbf{e}'_z$ directed along $[11\bar{2}]$, $[\bar{1}10]$, and $[111]$, correspondingly. The transformation is specified by the rotation

$$\begin{bmatrix}\mathbf{e}'_x\\ \mathbf{e}'_y\\ \mathbf{e}'_z\end{bmatrix}=\frac{1}{\sqrt{6}}\begin{bmatrix}1 & 1 & -2\\ -\sqrt{3} & \sqrt{3} & 0\\ \sqrt{2} & \sqrt{2} & \sqrt{2}\end{bmatrix}\begin{bmatrix}\mathbf{e}_x\\ \mathbf{e}_y\\ \mathbf{e}_z\end{bmatrix}. \tag{B1}$$

For simplicity we do not consider the strain part H_ε of the Hamiltonian since it is directly related to $H_{\mathbf{k}}$ by Eq. (6).

The *spherical* components of Hamiltonian in Eq. (2), proportional to unity matrix I and scalar products $\mathbf{L}\cdot\boldsymbol{\sigma}$ and $(\mathbf{L}\cdot\mathbf{k})^2$, are invariant under rotation and should be expressed in terms of the ladder operators for the sake of comparison with Eq. (3):

$$\mathbf{L}\cdot\boldsymbol{\sigma}=L_z\sigma_z+\sqrt{2}(L_+\sigma_-+L_-\sigma_+), \tag{B2}$$

$$(\mathbf{L}\cdot\mathbf{k})^2=k_\perp^2+L_z^2(k_z^2-k_\perp^2/2)+(L_+^2k_-^2+L_-^2k_+^2)/2 + \sqrt{2}([L_zL_+]k_zk_-+[L_zL_-]k_zk_+). \tag{B3}$$

The *warping* part of Eq. (2) is proportional to the combination $6[L_xL_y]k_xk_y+\text{c.p.}$, which under the rotation specified by Eq. (B1) transforms to the sums

$$(-2k_z^2+k_\perp^2)I+3(k_z^2-k_\perp^2/2)L_z^2+(L_+^2k_-^2+L_-^2k_+^2) + \sqrt{2}([L_zL_+]k_zk_-+[L_zL_-]k_zk_+) \tag{B4}$$

and

$$\sqrt{2}(L_+^2k_zk_++L_-^2k_zk_-)+([L_zL_+]k_+^2+[L_zL_-]k_-^2). \tag{B5}$$

A comparison of terms in Eqs. (B2)–(B4) of the transformed cubic equation with Eq. (3) for the wurtzite Hamiltonian leads to the cubic approximation in Eqs. (8) and (9). However, the warping terms in Eq. (B5), proportional to the difference $\gamma_2-\gamma_3$, do not have counterparts in the wurtzite Hamiltonian since the group C_{6v} is not a subset of cubic point groups.[19,26]

In the notations of Bir and Pikus, the quasicubic approximation for band-curvature parameters takes the form

$$A_2-A_1=-2A_4=A_3,\quad A_3=4A_5-\sqrt{2}A_6. \tag{B6}$$

Equation (B6) corrects the erroneous relation[38] $-A_3=4A_5-\sqrt{2}A_6$ used in a number of publications.

APPENDIX C: BLOCH FUNCTIONS SETS

The products of basis functions of angular momenta 1 and 1/2 are related to the basis functions of momenta $\frac{3}{2}$ and $\frac{1}{2}$ by means of vector addition (Clebsch-Gordan) coefficients[39]

$$\begin{bmatrix}\left|\frac{3}{2},\pm\frac{3}{2}\right\rangle\\ \left|\frac{3}{2},\pm\frac{1}{2}\right\rangle\\ \left|\frac{1}{2},\pm\frac{1}{2}\right\rangle\end{bmatrix}=\begin{bmatrix}1 & 0 & 0\\ 0 & \frac{1}{\sqrt{3}} & \sqrt{\frac{2}{3}}\\ 0 & \pm\sqrt{\frac{2}{3}} & \mp\frac{1}{\sqrt{3}}\end{bmatrix}\begin{bmatrix}|1,\pm1\rangle\left|\uparrow\atop\downarrow\right\rangle\\ |1,\pm1\rangle\left|\downarrow\atop\uparrow\right\rangle\\ |1,0\rangle\left|\uparrow\atop\downarrow\right\rangle\end{bmatrix}. \tag{C1}$$

Equation (C1) provides relations between different Bloch function sets, independent of their particular representation. If such representation is needed, the following form can be used for the functions $|1,m\rangle$:

$$|1,\pm1\rangle=(\mp|X\rangle-i|Y\rangle)/\sqrt{2},\quad |1,0\rangle=|Z\rangle, \tag{C2}$$

where $|X\rangle$, $|Y\rangle$, and $|Z\rangle$, are functions that transform as x, y, and z under operations of the point group. Unlike for cubic symmetry, the point group C_{6v} does not contain a horizontal reflection plane and the function $|Z\rangle$ is not odd in z. However, the even part of $|Z\rangle$ is proportional to a splitting constant $k_s\equiv m_0A_7/\hbar^2$ in Eq. (3) that is usually small.

According to the Wigner-Eckard theorem,[39] all matrix elements of vector $\hat{\mathbf{p}}$, $\langle L',m'|\hat{\mathbf{p}}|L,m\rangle$, calculated with different eigenstates of angular momenta L and L', can be expressed in terms of a single *reduced* matrix element $\langle L'||p||L\rangle$. The reduced matrix element for transitions between the eigenstates of $L=1$ and $L'=0$ is related to the commonly used quantity $P\equiv\langle Z|p_z|S\rangle$ by the equality $\langle1||p||0\rangle=\sqrt{3}P$. In this case all nonzero matrix elements are given by[39]

$$\langle S|\hat{p}_z|0\rangle=P,\quad \langle S|\hat{p}_+|-1\rangle=-\langle S|\hat{p}_-|1\rangle=\sqrt{2}P.$$

The lowering of symmetry from the spherical to the axial one leads to Eq. (42).

[1] *Properties of Group III Nitrides*, edited by J. H. Edgar, Electronic Materials Information Service Datareviews Series (Institution of Electrical Engineers, London, 1994).

[2] H. Morkoç *et al.*, J. Appl. Phys. **76**, 1363 (1994).

[3] S. Strite, Festkörperprobleme **34**, 79 (1994); S. Strite, M.-E. Lin, and H. Morcoç, Thin Solid Films **231**, 197 (1993).

[4] R. F. Davis, Proc. IEEE **79**, 702 (1992).

[5] H. Amano *et al.*, Appl. Phys. Lett. **48**, 353 (1986).

[6] H. Amano *et al.*, Jpn. J. Appl. Phys. **28**, L2112 (1989); S. Nakamura *et al.*, *ibid.* **31**, 1258 (1992).

[7] S. Nakamura *et al.*, Jpn. J. Appl. Phys. **30**, L1998 (1991); B. Goldenberg *et al.*, Appl. Phys. Lett. **62**, 381 (1993); M. A. Khan

et al., *ibid.* **66**, 2047 (1995); V. A. Dmitriev *et al.*, *ibid.* **68**, 229 (1996).

[8] S. Itoh *et al.*, Jpn. J. Appl. Phys. **32**, L1530 (1993); S. Nakamura *et al.*, *ibid.* **34**, L797 (1995); **34**, L1332 (1995); H. Sakai *et al.*, *ibid.* **34**, L1429 (1995); R. J. Molnar *et al.*, Appl. Phys. Lett. **66**, 268 (1995).

[9] R. L. Aggarwal *et al.*, J. Appl. Phys. **79**, 2148 (1996); S. Nakamura *et al.*, Jpn. J. Appl. Phys. **35**, L74 (1996).

[10] M. A. Khan *et al.*, SPIE Proc. **2149**, 254 (1994).

[11] M. A. Khan *et al.*, Appl. Phys. Lett. **62**, 1786 (1993); **63**, 214 (1993); V. A. Dmiriev *et al.*, *ibid.* **67**, 115 (1995); P. Shah *et al.*, J. Appl. Phys. **79**, 2755 (1996).

[12] S. Logothetidis *et al.*, Phys. Rev. B **50**, 18 017 (1994); J. Petalas *et al.*, *ibid.* **52**, 8082 (1995); R. Klann *et al.*, *ibid.* **52**, R11 615 (1995); R. Heitz *et al.*, *ibid.* **52**, 16 508 (1995); S. Kim *et al.*, *ibid.* **67**, 380 (1995); C. I. Harris *et al.*, *ibid.* **67**, 840 (1995); L. Eckey *et al.*, *ibid.* **68**, 415 (1996); T. J. Schmidt *et al.*, *ibid.* **68**, 1820 (1996); G. D. Chen *et al.*, *ibid.* **68**, 2784 (1996); A. V. Andrianov *et al.*, Semicond. Sci. Technol. **11**, 366 (1996); S. Chichibu *et al.*, J. Appl. Phys. **79**, 2784 (1996); W. Shan *et al.*, *ibid.* **79**, 3691 (1996); J. Miragliotta and D. K. Wickenden, Phys. Rev. B **53**, 1388 (1996); J. Menniger *et al.*, *ibid.* **53**, 1881 (1996).

[13] T. L. Tansley and R. J. Egan, Physica B **185**, 190 (1993); A. Salvador *et al.*, Appl. Phys. Lett. **67**, 3322 (1995); P. Perlin *et al.*, Phys. Rev. Lett. **75**, 296 (1995); C. Wetzel *et al.*, Phys. Rev. B **53**, 1322 (1996).

[14] M. Rubin *et al.*, Appl. Phys. Lett. **64**, 64 (1994); C. Johnson *et al.*, *ibid.* **68**, 1806 (1996).

[15] Y.-N. Xu and W. Y. Ching, Phys. Rev. B **48**, 4335 (1993); K. Miwa and A. Fukumoto, *ibid.* **48**, 7897 (1993); N. E. Christensen and I. Gorczyca, *ibid.* **50**, 4397 (1994); A. F. Wright and J. S. Nelson, *ibid.* **51**, 7866 (1995); W. R. L. Lambrecht *et al.*, *ibid.* **51**, 13 516 (1995); T. Yang *et al.*, Jpn. J. Appl. Phys. **34**, 5912 (1995); J. Neugebauer and C. G. Van de Walle, Phys. Rev. Lett. **75**, 4452 (1995); W. J. Fan *et al.*, J. Appl. Phys. **79**, 188 (1996); Solid State Commun. **97**, 381 (1996).

[16] K. Kim, W. R. L. Lambrecht, and B. Segall, Phys. Rev. B **50**, 1502 (1994); *ibid.* **53**, 16 310 (1996); in *Gallium Nitride and Related Materials*, edited by R. D. Dupuis, J. A. Edmond, F. A. Ponce, and S. Nakamura, MRS Symposia Proceedings No. 395 (Materials Research Society, Pittsburgh, 1996), p. 399; W. R. L. Lambrecht, K. Kim, S. N. Rashkeev, and B. Segall, *ibid.* p. 455.

[17] M. A. Littlejohn *et al.*, Appl. Phys. Lett. **26**, 625 (1975); R. P. Joshi, *ibid.* **64**, 223 (1994); N. S. Mansour *et al.*, J. Appl. Phys. **77**, 2834 (1995); J. Kolnik *et al.*, *ibid.* **78**, 1033 (1995).

[18] W. Fang and S. L. Chuang, Appl. Phys. Lett. **67**, 751 (1995); W. W. Chow, A. Knorr, and S. W. Koch, *ibid.* **67**, 754 (1995); W. W. Chow, A. F. Wright, and J. S. Nelson, *ibid.* **68**, 298 (1996).

[19] G. L. Bir and G. E. Pikus, *Symmetry and Strain-Induced Effects in Semiconductors* (Wiley, New York, 1974).

[20] E. L. Ivchenko and G. E. Pikus, *Superlattices and Other Heterostructures: Symmetry and Optical Phenomena* (Springer, Berlin, 1995).

[21] J. M. Luttinger and W. Kohn, Phys. Rev. **97**, 869 (1955).

[22] J. M. Luttinger, Phys. Rev. **102**, 1030 (1956).

[23] E. I. Rashba, Fiz. Tverd. Tela (Leningrad) **1**, 407 (1959) [Sov. Phys. Solid State **1**, 368 (1959)]; E. I. Rashba and V. I. Sheka, *Fiz. Tverd. Tela (Leningrad), Collection of papers II* (Acad. Sci. USSR, Moscow, 1959), p. 162.

[24] G. E. Pikus, Zh. Éksp. Teor. Fiz. **41**, 1258 (1961) [Sov. Phys. JETP **14**, 898 (1962)]; **41**, 1507 (1961) [**14**, 1075 (1962)].

[25] M. Ueta, H. Kanzaki, K. Kobayashi, Y. Toyozawa, and E. Hanamura, *Excitonic Processes in Solids* (Springer, Berlin, 1986).

[26] K. Cho, Phys. Rev. B **14**, 4463 (1976).

[27] G. L. Bir, G. E. Pikus, L. G. Suslina, D. L. Fedorov, and E. B. Shadrin, Fiz. Tverd. Tela (Leningrad) **13**, 3551 (1971) [Sov. Phys. Solid State **13**, 3000 (1971)].

[28] R. C. Casella, Phys. Rev. Lett. **5**, 371 (1960); E. I. Rashba, Fiz. Tverd. Tela (Leningrad) **2**, 1224 (1960) [Sov. Phys. Solid State **2**, 1109 (1960)]; G. D. Mahan and J. J. Hopfield, Phys. Rev. **135**, A428 (1964); L. C. Voon *et al.*, Phys. Rev. B **53**, 10 703 (1996).

[29] D. W. Langer, R. N. Euwema, K. Era, and T. Koda, Phys. Rev. **2**, 4005 (1970).

[30] S. Ninomiya and S. Adachi, J. Appl. Phys. **78**, 4681 (1995).

[31] M. Suzuki, T. Uenoyama, and A. Yanase, Phys. Rev. B **52**, 8132 (1995).

[32] T. Uenoyama and M. Suzuki, Appl. Phys. Lett. **67**, 2527 (1995).

[33] Yu. M. Sirenko, J.-B. Jeon, K. W. Kim, M. A. Littlejohn, and M. A. Stroscio, Phys. Rev. B **53**, 1997 (1996).

[34] S. L. Chuang and C. S. Chang, Appl. Phys. Lett. **68**, 1657 (1996).

[35] J.-B. Jeon, Yu. M. Sirenko, K. W. Kim, M. A. Littlejohn, and M. A. Stroscio, Solid State Commun. **99**, 423 (1996).

[36] Yu. M. Sirenko, J.-B. Jeon, K. W. Kim, M. A. Littlejohn, and M. A. Stroscio, Appl. Phys. Lett. **69**, 2504 (1996).

[37] J. J. Hopfield, J. Phys. Chem. Solids **15**, 97 (1960).

[38] The error takes place at the final stage of derivation. From expressions $A_3=A_3'$, $A_5=(A_2'+2A_3')/6$, and $A_6=(2A_2'+A_3')/3\sqrt{2}$ on pp. 329 and 330 of Ref. 19, it follows that $4A_5-\sqrt{2}A_6=+A_3$, instead of incorrect result $4A_5-\sqrt{2}A_6=-A_3$ in Eq. (31.13) of Ref. 19.

[39] L. D. Landau and E. M. Lifshits, *Quantum Mechanics* (Pergamon, Oxford, 1977).

[40] For representation of Eqs. (2) and (3) one can use any set of 3×3 matrices L_i satisfying the relation $L_iL_j-L_jL_i=i\varepsilon_{ijk}L_k$. We employ the quantum-mechanical definition (Refs. 39, 24, 27, 33, and 20) of L_i, which is related to matrices L' used in Refs. 19 and 31 as $L_x'=L_y$, $L_y'=-L_x$, and $L_z'=L_z$. Corresponding ladder operators (Refs. 19 and 31) are given by $L_\pm'\equiv\pm i(L_x'\pm iL_y')/\sqrt{2}=L_\pm$.

[41] W. P. Mason, *Physical Acoustics and the Properties of Solids* (Van Nostrand, New York, 1958).

[42] D. A. Broido and L. J. Sham, Phys. Rev. B **31**, 888 (1985).

[43] C. Y.-P. Chao and S. L. Chuang, Phys. Rev. B **46**, 4110 (1992).

[44] V. F. Gantmakher and I. B. Levinson, *Carrier Scattering in Metals and Semiconductors* (Elsevier, Amsterdam, 1987).

[45] J. D. Wiley, Phys. Rev. B **4**, 2485 (1971); F. Szmulowicz, *ibid.* **28**, 5943 (1983); M. Woerner and T. Elsaesser, *ibid.* **51**, 17 490 (1995); D. Ahn, J. Appl. Phys. **78**, 4505 (1995); K. Yeom, J. M. Hinckley, and J. Singh, *ibid.* **79**, 2790 (1996).

[46] This term, however, contributes for optical *intersubband* transitions in confined structures: see, e.g., L. C. West and S. J. Eglash, Appl. Phys. Lett. **46**, 1156 (1985).

[47] S. W. Corzine, R.-H. Yan, and L. A. Coldren, in *Quantum Well Lasers*, edited by P. S. Zory, Jr. (Academic, Boston, 1993).

[48] Y.-C. Chang and R. B. James, Phys. Rev. B **39**, 12 672 (1989); E. V. Bakhanova and F. T. Vasko, Phys. Status Solidi B **182**, 97 (1994).

[49] F. Szmulowicz, Phys. Rev. B **51**, 1613 (1995).

[50] B. Gil, O. Briot, and R.-L. Aulombard, Phys. Rev. B **52**, R17 028 (1995).

[51] Since the sign of the band-curvature parameter A_5 is not determined by the hole spectrum at $k_z=0$ and/or $k_\perp=0$, we changed

the sign of A_5 in Ref. 31 to comply with the correct form of quasicubic approximation in Eq. (B6).

[52] A. Polian, M. Grimsditch, and I. Grzegory, J. Appl. Phys. **79**, 3343 (1996).

[53] G. Dresselhaus, A. F. Kip, and C. Kittel, Phys. Rev. **98**, 368 (1955).

[54] E. O. Kane, Phys. Rev. **178**, 1368 (1969).

[55] W. H. Kleiner and L. Roth, Phys. Rev. Lett. **2**, 234 (1959).